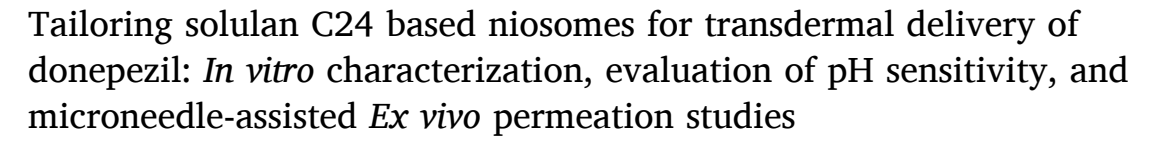
Contents lists available at ScienceDirect

## Journal of Drug Delivery Science and Technology

journal homepage: www.elsevier.com/locate/jddst



## Research paper



Archana S. Nayak a, Srivani Chodisetti a, Shivaprasad Gadag b, Usha Yogendra Navak b, Srinikethan Govindan<sup>a</sup>, Keyur Raval<sup>a,\*</sup>

- <sup>a</sup> Department of Chemical Engineering, National Institute of Technology Karnataka, Surathkal, Mangalore, 575025, India
- b Department of Pharmaceutics, Manipal College of Pharmaceutical Sciences, Manipal Academy of Higher Education, Manipal, Karnataka, 576104, India

#### ARTICLE INFO

#### Keywords: pH-sensitive donepezil niosome Thin film hydration Gas chromatography Kinetic modeling Microneedle-assisted Transdermal permeation

#### ABSTRACT

The present investigation aims at encapsulating donepezil (DNP) in a niosomes to avert the side effects and to deliver the intact carrier across the skin barrier by modulating its physicochemical properties. The finding conclusively demonstrated that entrapment efficiency and the alteration in the niosome size are associated with the change in the span 60: cholesterol ratio, sonication, and hydration volume. The addition of 5 mM of solulan C24 to the optimized formulation (NSV5<sub>SolC24</sub>) formed stable niosomes with a mean particle size of  $180.1 \pm 1.83$ nm and entrapment efficiency of 82.15%  $\pm$  1.54%. The cryo-SEM image and in vitro drug release profile revealed that the NSV5<sub>SolC24</sub> is pH-sensitive. FTIR spectral analysis of NSV5<sub>SolC24</sub> suggested that the ether and ester group in the NSV5<sub>SolC24</sub> complex undergoes S<sub>N</sub>2 cleavage and hydrolysis at lower pH, thus enhancing DNP release. The microneedle (MN)-assisted studies with MN1200 showed a 29-fold increase in transdermal permeation of intact  $NSV5_{SolC24}$  against the passive method in porcine skin. The intact  $NSV5_{SolC24}$  carrying DNP was translocated across the skin barrier successfully at a steady flux rate of  $9.89 \pm 0.923 \,\mu\text{g/cm}^2\text{/h}$ . Nevertheless, further in vivo studies are recommended to elucidate the pH sensitivity and clinical efficacy of the prepared drug delivery system.

## 1. Introduction

Alzheimer's disease (AD) is a multifactorial progressive neurological disorder, principally characterized by cognitive and behavioral abnormalities due to cholinergic dysfunction. Thus, restoration of cholinergic neurotransmission may help to ameliorate impaired memory in AD patients [1]. Donepezil (DNP), a cholinesterase inhibitor, is known to reduce/prevent rapid hydrolysis of acetylcholine esterase and restore cholinergic synapses [2]. Although DNP is not a permanent cure, encouraging results were obtained by significantly improving the intellectual capacity of AD patients on oral administration of film-coated tablets of 5-10 mg dosage per day [3,4].

A successful oral administration, however, is not pragmatic in patients with impaired cognitive function [5]. The patient may either skip or overdose with the drug. Overdosing may lead to the accumulation of the drug in the systemic circulation (half-life, t<sub>1/2</sub>: 70h), thereby escalating DNP concentration above its therapeutic level. The oral intake of DNP is known to increase gastric acid secretion and lead to adverse effects due to the non-specific interaction of DNP with the peripheral cholinergic nerves [2,6]. Hence many attempts were made to deliver DNP to the brain through alternate route and delivery systems. Reports suggested that nasal delivery of DNP in chitosan nanosuspension [7], liposome [8], thiolate-chitosan hydrogel [9], and solid lipid nanoparticle [10] enhanced the mean DNP content in the brain. The nasal route bypasses the limitation of the blood-brain barrier (BBB) as there is a unique connection between the olfactory lobes and the brain. However, the quantity of the drug delivered does not exceed beyond 0.01%-0.1% at the nanomolar level due to limited surface area, and the presence of the mucous layer negates the bioavailability [11]. Also, the intravenous administration of polysorbate coated DNP- poly lactic-co-glycolic acid (PLGA) nanoparticles significantly improved the specificity to target the brain [12]. Undoubtedly, the results demonstrated by the nanoparticle were promising in brain targeted delivery. However, the patient's compliance with the prescribed dosage is a



<sup>\*</sup> Corresponding author. Department of Chemical Engineering, National Institute of TechnologyKarnataka, Surathkal, 575025, India. E-mail address: keyurnraval@nitk.edu.in (K. Raval).

critical bottleneck. Hence, the route of administration is pivotal while addressing AD patients.

Transdermal administration of DNP was well tolerated in healthy human subjects and proven to be an effective route for the administration of DNP [13]. The use of chemical enhancers in a transdermal system is known to promote drug permeation. The non-ionic surfactant, Brij®30, combined with Brij®52 in an acrylic rubber matrix, is an exemplar for increased DNP permeation [14]. The literature emphasizes that the microneedle (MN) system, which is minimally invasive, can be used in overcoming the skin barrier and enhance transdermal delivery of the drug, including macromolecules [15-18]. Synthesis of hydrogel MNs (600  $\mu m$ ) integrated with the plasticized film of DNP emerged as a promising prototype for transdermal delivery of the drug across the porcine skin with a steady release of 854.71  $\pm$  122.71  $\mu g$  of DNP over 24 h [19]. The dissolving microneedle tip of DNP in combination with (HPMC)-ethanol/water hydroxy-propyl-methyl-cellulose demonstrated good mechanical strength when inserted into porcine skin and 95% of the drug was released after 5 min of insertion [20]. The reports suggested that MN-assisted transdermal delivery can stand in lieu of oral dosage.

Undoubtedly, the MNs, coupled with chemical enhancers, can boost the drug permeation across the skin barrier and facilitate systemic absorption of the drug. However, if the drug is intended for the skin to brain delivery, then the drug must be encapsulated in a carrier that can breach the skin barrier and then release the drug at the target site based on either the stimulus-response model or receptor-mediated targeting [21]. This unique challenge can be effectively tackled by applying MNs with a hollow bore to disrupt the physical barrier [15,18] and dispense the nanocarriers to the viable epidermis, which can then navigate in the systemic circulation to reach the target site.

To date, there are no studies reported on transdermal delivery of intact DNP loaded nanocarrier to target the brain. Among the nanocarrier, niosomes composed of non-ionic surfactants have received significant attention in recent years as a promising drug delivery system due to its chemical and biological stability and that its ability to deliver the drug across the skin barrier [22–26]. Hence, the present study focusses on the synthesis of stable niosomes by modulating the process and formulation variable to explore its interdependence on the physicochemical properties and investigate its effect on MN-assisted permeation.

Furthermore, the structural transition of  $A\beta$  amyloids by Cu (II) in the AD brain alters the physiological pH between 6.6 and 6.8 inducing cerebral acidosis [27,28]. Hence developing a pH-sensitive carrier (response-stimulus model) that can bypass the skin and reach systemic circulation can pave the way for site-directed drug delivery. Reports revealed that the addition of surfactant, Solulan<sup>TM</sup> C24 (Sol C24), a lanolin derivative emulsifier, into the niosomal formulation improves the membrane fluidity and elasticity to produce a homogenous spherical niosomes [29–32]. Sol C24 is a complex of ethoxylated cholesterol and ethoxylated vegetable fatty alcohol with ether as one of the functional groups. Theoretically, at acidic pH, ether undergoes acidic cleavage by an  $S_N 2$  mechanism [33,34]. Hence, we assume that the addition of Sol C24 to the niosome could impart pH sensitivity and aid in drug release at lower pH.

Consistent with this concept, the present investigation emphasizes on evaluating the process and formulation parameters that critically affected the physicochemical properties of the niosomes. The optimized niosomal formulation with membrane additive is assessed for pH sensitivity by *in vitro* release kinetic studies, scanning electron microscope (SEM) imaging, and Fourier-transform infrared spectroscopy (FTIR). The feasibility of MN-assisted transdermal delivery of intact DNP niosomes across porcine skin is also investigated.

#### 2. Materials and methods

#### 2.1. Chemicals

Span 60 (S60), Cholesterol (CHOL) ≥99% purity, and Dicetyl Phosphate (DCP) were procured from Sigma Aldrich. Donepezil hydrochloride (DNP) >98%, HPLC grade, and Phosphate Saline Buffer (PBS) (10X) were purchased from TCI and Himedia, respectively. Solulan C24 (Sol C24), a lanolin derivative, was a generous gift from Lubrizol (Brussel, Belgium). The organic solvent used were of analytical grade.

## 2.1.1. Simulated body fluid (SBF) preparation

SBF was prepared by adding NaCl: 8.035g, NaHCO $_3$ :0.355g, KCl: 0.225g, K $_2$ HPO $_4$ .3H $_2$ O: 0.231g, MgCl $_2$ .6H $_2$ O: 0.311g, 1.0 M HCl: 39 ml, CaCl $_2$ : 0.292g, Na $_2$ SO $_4$ : 0.072g in 700 ml of ion-exchanged distilled water. The pH of the obtained solution is 2.0  $\pm$  1.0. Tris (tris-hydroxyl methyl aminomethane): 6.118g was slowly added to get a solution of pH 7.45  $\pm$  0.01 and made up to 1000 ml. The pH was adjusted to 5.4, 6.8, and 7.4 using 1 N HCl/NaOH to stimulate the skin, brain, and body fluid, respectively [35].

#### 2.2. Methods

#### 2.2.1. Formulation of DNP loaded niosomes

The conventional thin-film hydration (TFH) method was employed to synthesize niosomes. Accurately weighed quantities the drug DNP, S60, CHOL, and the membrane additives (DCP/Sol C24) were dissolved in chloroform (CHCl<sub>3</sub>) in the round bottom flask (Table 1), and the solvent was evaporated under vacuum at 60 °C using a rotary flash evaporator (Buchi Rotavapor® R-215, Bangalore, India).

The thin film layer, once formed, was then subjected to vacuum to remove the residual CHCl $_3$  under the inert environment, which was then hydrated for 45 min with PBS (pH 7.4) under rotation at 65 °C (above the phase transition temperature,  $T_c$ ) [36,37]. The formulation was then subjected to sonication (20 kHz, 40% amplitude, 500W Ultrasonic Probe Ultrasonicator, India) based on the experimental design. During sonication, the niosomal suspension container was covered by aluminum foil to prevent evaporative loss and immersed in the ice-salt bath to diminish temperature-driven side effects. The sonicator was operated in pulsed mode to retard the rate of temperature increase and to allow for better temperature control.

## 2.2.2. Gas chromatography for analysis of CHCl3 in thin film

The thin film layer was analyzed for traces of CHCl $_3$  by gas chromatography (Trace Ultra, DB-5 column: 30 m  $\times$  0.25 mm x 0.25 µm, Detector: Electron capture detector, Auxillary detector: Flame ionization detector, carrier gas flow rate: 1.2 ml/min and acquisition time: 16 min). Thin-film prepared was subjected to vacuum for 0, 3, and 12 h. The thin film was then dissolved in carbon tetrachloride (CCl $_4$ ) and analyzed for residual CHCl $_3$ . CCl $_4$  was selected as a solvent-based on its miscibility with CHCl $_3$  and the difference in retention times.

## 2.2.3. Physicochemical characterization of niosomes

The mean particle size, zeta potential, and PDI of the formulation were estimated by differential light scattering at  $25\,^{\circ}$ C using Zetasizer (Malvern Instruments, UK). PDI is the determinant of the degree of homogeneity [37]. The surface morphology was studied using scanning electron microscopy (SEM, JEOL/JSM 6380, LA), cryo-SEM (JEOL/JSM 7600, Quorum PP3000T, Japan) and high-resolution transmission electron microscope (HR-TEM, Jeol/JEM 2100, LaB6).

## 2.2.4. Determination of entrapment efficiency

The intact DNP loaded niosomes were purified by Sephadex G50 mini-column centrifugation technique with suitable modifications [38, 39]. 250  $\mu$ l of PBS of pH 7.4 was added to the column and centrifuged at 200xg for 10 min (Remi C-24 plus, Bangalore, India) to replace the water

**Table 1**The composition of niosomal formulation<sup>a</sup>.

Formulation Code	S60 (mM)	CHOL (mM)	S60: CHOL	Formulation Code	S60 (mM)	CHOL (mM)	S60: CHOL
NSV1	0	10	0	NCV1	10	0	_
NSV2	3	10	0.3	NCV2	10	3	3.33
NSV3	6	10	0.6	NCV3	10	6	1.66
NSV4	9	10	0.9	NCV4	10	9	1.11
NSV5	12	10	1.2	NCV5	10	12	0.83
NSV6	15	10	1.5	NCV6	10	15	0.66
NSV7	18	10	1.8	NCV7	10	18	0.55
NSV8	21	10	2.1	NCV8	10	21	0.47
NSV9	24	10	2.4	NCV9	10	24	0.41
NSV10	27	10	2.7	NCV10	10	27	0.37

<sup>&</sup>lt;sup>a</sup> Constant Parameter: DNP loading: 5 mg, Hydration Time: 45 min, and Hydration Volume: 10 ml.

in the resin. Approximately 200  $\mu l$  of DNP free niosomes were loaded over the Sephadex G50 resin and centrifuged again for pre-saturation. DNP loaded niosomes were then added to the column, followed by centrifugation to evade void volume and remove non-associated DNP. The resin was then eluted with PBS thrice. The eluate was combined with an equal amount of 100% methanol to facilitate the disruption of the niosomes and complete solubilization of the DNP. Solvent treated niosomal suspension was then subjected to centrifugation at 21000xg at 4  $^{\circ}\text{C}$  for 30 min.

The amount of DNP in the supernatant was quantified using the RP-HPLC system (Waters e2695 system) consisting of a UV detector (Waters 2489 UV/Vis Detector) [40]. Phenyl RP column (25 cm  $\times$  4.6 mm, 5  $\mu$ ) set at 40 °C was used as the stationary phase. The separation was achieved using a solvent mixture of methanol:20 mM phosphate buffer (pH 7.4): triethylamine (60: 40: 0.5, v/v) as the mobile phase by isocratic elution at the flow rate of 1 ml/min. The wavelength of the UV detector was tuned to 268 nm, and 20  $\mu$ l of the filtered, degassed sample was injected. The peaks for DNP were detected at a retention time of 6.8 min and compared with the standard calibration curve. Entrapment efficiency was calculated based on the equation given below.

$$Entrapment\ Efficiency = \frac{DNP\ entrapped}{Total\ DNP\ loaded} \times 100 \tag{1}$$

#### 2.2.5. In vitro drug release studies and kinetic modeling

The *in vitro* release studies from the niosomes were carried out by bulk-equilibrium reverse dialysis method to prevent drug saturation using a visking tube in different pH medium [41,42]. The release mediums SBF 5.4, SBF 6.8, and SBF 7.4 were maintained at 37 °C with a stirring speed of 100 rpm to simulate the pH of the skin, brain, and blood plasma, respectively. Dialysis membrane (Dialysis membrane 110, LA-395, Himedia) of 12k-14kDa MWCO was equilibrated with 3 ml of release medium of different pH (receiver compartment-visking tube) and placed in the donor compartment for 12 h before the experiment. 5 ml of the DNP-loaded niosomes was added directly into 500 ml of the donor compartment. At a regular interval, samples were withdrawn from the visking tube and replenished with the fresh SBF medium of appropriate pH. The samples withdrawn were treated with an equal volume of 100% methanol, and DNP content was determined by the HPLC method. Cumulative DNP release percentage was calculated as:

$$Q = \frac{(V_o C_t) + V \sum_{n=1}^{t-1} C}{W} \times 100$$
 (2)

Where Q,  $V_0$ ,  $C_t$ , V, C, and, W were a cumulative percentage of drug released, the total volume of release medium, DNP concentration at time t, the volume of release medium withdrawn at each interval, cumulative DNP concentration and weight of the total drug, respectively.

The data obtained were fitted into time-dependent model equations such as zero-order, first-order, Higuchi, Hixson-Crowell, and Korsmeyer-Peppas model to assess the mechanism of drug release. Linear regression analysis of the above curves determined the  $\rm r^2$  values and release

exponent (n) value from the Korsmeyer-Peppas model defined the release mechanism.

#### 2.2.6. Evaluation of pH sensitivity

The optimized blank niosomes were purified by mini-column centrifugation and were eluted by PBS. The eluate was then adjusted to pH 7.4, 6.8, and 5.4 using HCl and NaOH and then lyophilized (FD5 series Freeze Dryer, Bangalore, India) to comprehend the effect of pH on the niosome structure. The IR spectra of the freeze-dried niosomes were recorded using FTIR (Bruker Alpha II, Bangalore, India) operated in attenuated total reflection (ATR) mode with 12 scans in the wavelength range of 4000 cm<sup>-1</sup> to 500 cm<sup>-1</sup> and resolution of 4 cm<sup>-1</sup> to study their possible interactions. Also, the morphological changes in the niosomes with the change in pH at hydrated conditions were captured using field emission gun (FEG) -SEM (Jeol/JSM 7600, Japan) equipped with the cryo unit (Quorum, PP3000t, UK).

## 2.2.7. Ex-vivo permeation studies of niosomes through MN

White porcine ear auricles were obtained from the abattoir for transdermal permeation studies as a substitute for human skin due to its permeability characteristics and its histological and biochemical similarities [43,44]. Ear epidermis was separated using a scalpel, and excess subcutaneous fat was removed carefully. The skin was then mounted on jacketed vertical Franz diffusion cell (Orchid Scientific, Nasik, India) and clamped between the receptor (20 ml of 20 mM PBS, pH 7.4) and donor cell (2 ml) with its stratum cornea facing towards the donor cell. The stirring speed of the receptor cell was fixed to 600 rpm, and the permeation studies were carried out at 32  $\pm$  0.5 °C using a temperature-controlled water circulation system. The surface area of 2.5 cm² was available for permeation. DNP concentration equivalent to 1.66 mg/ml was loaded in the donor cell either in the form of free DNP in PBS or as DNP loaded in niosomes based on the experimental design.

The permeation studies for niosomes were carried by the active method and then compared with the passive method [15,45]. The active method involved the application of MN array: 600, 777, and 1200 (AdminPatch® Microneedle Arrays, nanoBioScience LLC, CA, USA) individually on the skin by applying steady pressure, manually and then loaded with the DNP niosomes. The MN array system applied were kept undisturbed during permeation studies. Samples from the receptor cell were collected at an interval of 2, 4, 8, 12, and 24 h and replenished with the fresh medium. The sample was subjected to centrifugal filtration (Amicon® Ultra-3K device) at 5000xg for 10 min to remove the free DNP and residual niosomal components. The intact DNP niosomes were collected from the retentate, and an equal volume of methanol was added to disrupt the niosomes. The treated niosomal suspension was then subjected to centrifugation at 21000xg at 4 °C for 30 min (Remi C-24 plus, Bangalore, India). The free DNP in the supernatant was determined by HPLC analysis.

The permeation profile for intact niosomes carrying DNP as a function of time was plotted for both passive, and MN treated active method. Apparent permeation coefficient  $(K_p)$  was computed using Fick's first

law of diffusion:

$$\frac{1}{A}\left(dM_{/dt}\right) = J_s = K_p \Delta C \tag{3}$$

 $J_s$  is the flux (µg/cm²/h), M is the cumulative amount of drug in the intact niosome permeated across the skin (µg/cm²), A is the active area of the skin (2.5 cm²),  $K_p$  is the apparent permeability coefficient (cm/h), and  $\Delta C$  is the difference in concentrations of DNP in the donor and receiver.

Enhancement ratio (ER) was computed to evaluate the relative efficiency of different MN in translocating the intact niosomes across the skin. The enhancement ratios were calculated as:

Enhancement Ratio (ER) = 
$$\frac{Flux \ obtained \ after \ MN \ application}{Flux \ obtained \ without \ MN \ application}$$
(4)

#### 2.2.8. DNP content in porcine skin

The porcine skin was minced and homogenized (Omni Tissue Master 125 Homogenizer, Bangalore, India) in 50% methanol in PBS. The homogenate was centrifuged at 18700xg, and the supernatant was analyzed for DNP content by HPLC.

#### 2.2.9. Stability studies

Optimized DNP loaded niosomes stored in a refrigerator were subjected to long term and accelerated stability studies as per ICH Q1A(R2) (CPMP/ICH/2736/99) guidelines [46]. DNP loaded niosomes were stored in refrigeration and in a programmable chamber at 5 °C  $\pm$  3 °C and 25 °C  $\pm$  2 °C/60% RH  $\pm$  5%RH respectively. The samples were drawn at a regular time interval and assessed for changes in mean particle size, PDI, zeta-potential, and entrapment efficiency to evaluate the stability of the formulation.

#### 2.2.10. Statistical analysis

Data obtained were analyzed with Origin Pro 8.0 and Microsoft Excel 2016 package. The experiments were carried out in triplicates, and the results were expressed as mean  $\pm$  SD. The group of data obtained was subjected to regression analysis to determine the *p-value*. The significance threshold of 0.05 was fixed.

#### 3. Results and discussion

In the present study, DNP niosomes were prepared and attempted to deliver through the MN approach across the skin. The suitability of any nanocarrier system depends on the physicochemical properties and stability. Hence, a framework to assess the characteristics of the niosome was designed by controlling the formulation and process variables.

Fig. 1 graphically illustrates the TFH method used to prepare the niosomes. The primary objective in this investigation was to determine the optimum experimental conditions which would yield the best responses, including mean particle size under 200 nm with excellent entrapment efficiency, homogeneity, and stability.

#### 3.1. Analysis for traces of CHCl<sub>3</sub> in the thin film by gas chromatography

Elimination of  $CHCl_3$  from the thin-film is a critical stage as it can destabilize the niosomes by solubilizing the membrane components and increase the cytotoxicity of the formulation. Reports suggested that placing the thin-film formed in a vacuum desiccator [47,48] or an inert nitrogen environment [36] overnight can effectively eliminate the residual  $CHCl_3$ . However, it is a time-consuming process that can exert influence on upscaling and production efficiency in an industrial setting. Hence, it is vitally important to curtail the process-time in the TFH method used for the synthesis of niosomes.

Accordingly, the thin film (S60-CHOL) formed by the solvent

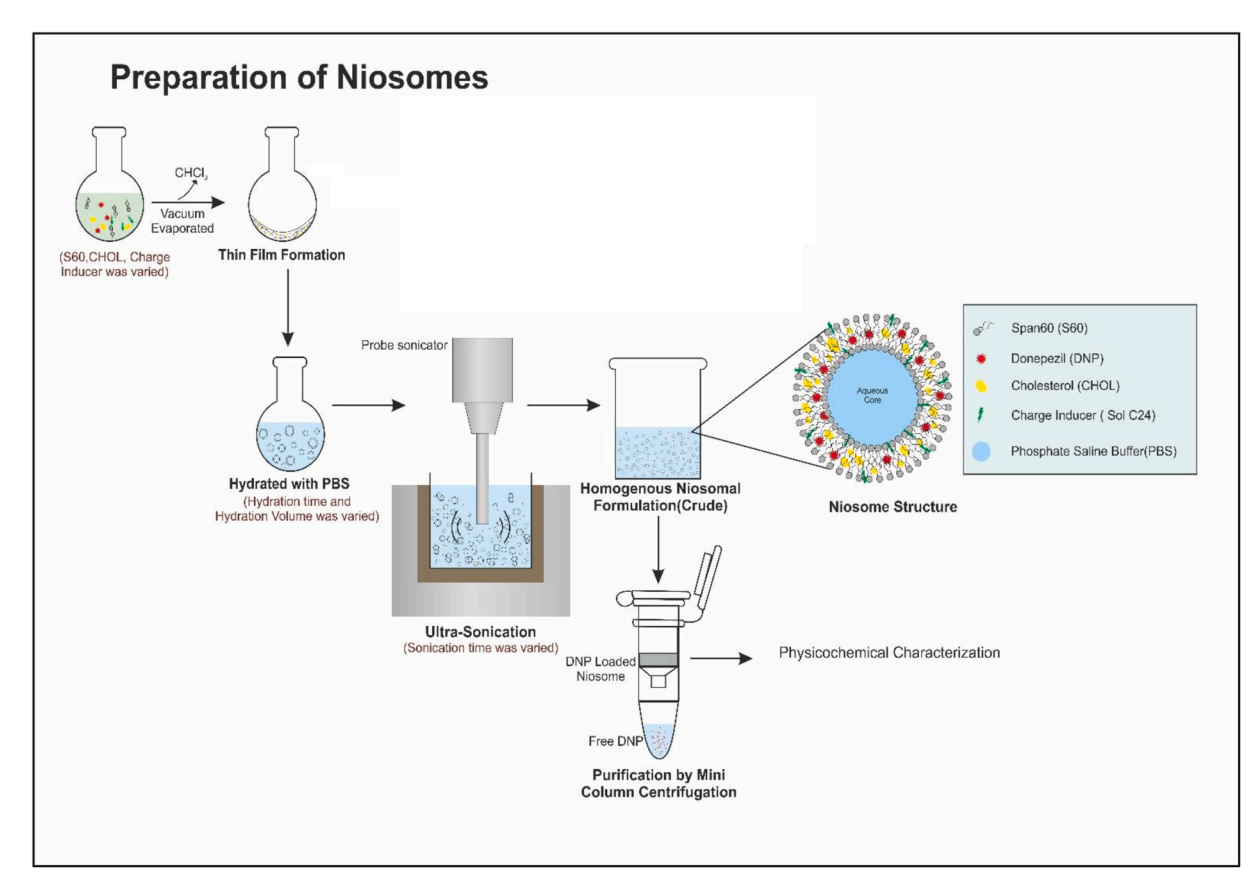


Fig. 1. Schematic representation of the TFH method employed to synthesize DNP niosomes.

evaporation was subjected to a vacuum for a discrete-time length to optimize the vacuum time. The thin-film deposited was then solubilized in  $\mathrm{CCl_4}$  based on its miscibility with  $\mathrm{CHCl_3}$  and distinct retention time. The resultant mixture was then analyzed for traces of  $\mathrm{CHCl_3}$  in  $\mathrm{CCl_4}$  by gas chromatography. The chromatogram obtained is presented in Fig. 2.

Both CHCl $_3$  and CCl $_4$  registered characteristic peaks at a retention time of 3.2 min and 3.6 min, respectively. Also, substantial changes in the peak were noted at different vacuum time. Analysis of the chromatogram showed that thin-film subjected to 3 h and 12 h of vacuum under inert environment showed no traces of CHCl $_3$ . However, at 0<sup>th</sup> h (after the formation of the thin film), a small peak of CHCl $_3$  was recorded at a retention time of 3.2 min (Fig. 2a). From the preliminary results, it appears that a vacuum time of 3 h is adequate to eliminate CHCl $_3$ , thus curtailing process time. On this basis, further formulations were synthesized by the TFH method with 3 h of vacuum time.

#### 3.2. Effect of S60 concentration

Ten different molar concentrations of surfactant, S60 was considered for the synthesis of niosomes, and S60 concentration was varied from 0 to 27 mM, as shown in Table 1. All the other parameters, such as DNP loading (5 mg), CHOL concentration (10 mM), hydration time (45 min), and hydration volume (10 ml), were kept constant in the study. Nonionic surfactant, S60 with a hydrophilic-lipophilic balance (HLB) value of about 4.7, was considered for the study owing to its hydrophobicity and high phase transition temperature ( $T_c = 53~^{\circ}C$ ), which enables better entrapment of the drug [49]. Over and above, S60 is an ester-linked surfactant which degrades into nontoxic triglycerides and fatty acid catalyzed by esterase [50] and hence biocompatible. As shown in Fig. 3, the variation in S60 concentration significantly affects the mean particle size and entrapment efficiency of the prepared niosomes, and the higher concentration of S60 resulted in smaller mean particle size and greater entrapment efficiency.

In this investigation, the mean particle size of the DNP loaded niosome reduced significantly (p <0.05) by 42% with an increase in S60 concentrations from 3 mM to 21 mM. The stability and the PDI of the formulation too improved with increasing S60 strength. NSV1 was not considered for physicochemical evaluation as no niosomes can be formed without non-ionic surfactant in the formulation.

At a lower concentration of S60 (NSV2 and NSV3), the surfactant molecules may not stabilize the membrane of the niosome [51,52], which could have led to the formation of a larger niosome and formed sediments on storage (Fig. 4 b,c). These niosomes thus formed were unstable. From the investigation, it was observed that when the concentration of CHOL is much higher than the S60 concentration, the excess CHOL precipitated out. The CHOL, which is represented by an inverted cone shape, acts as mortar in the bilayer and functions cooperatively with the surfactant monomers by virtue of its molecular shape to form stable niosomes. However, CHOL molecules are comparatively rigid molecules too and possess head groups too small to pack into an

organized conformation [53,54]. As a result, the excess CHOL precipitated due to its inability to accommodate the acyl chained lipid in the bilayer leading to the formation of unstable niosomes.

With further increase in S60 concentration, the transition of the S60-CHOL molecule from a dispersed lamellar layer to the vesicular system might have attributed to the formation of thermodynamically stable niosomes of smaller size [55] (Fig. 4 d,e). Additionally, the low HLB value of S60 and surface free energy leads to relatively less uptake of water in the core and thus forming smaller niosomes [56]. The NSV8 formulation with an S60 concentration of 21 mM recorded the smallest mean particle size of 264.25  $\pm$  6.4 nm. The formulations NSV4 to NSV7 showed a remarkable degree of homogeneity with PDI  $\leq$  0.5 and stability when stored at 4  $^{\circ}$ C for 30 days with no signs of sedimentation.

However, beyond the S60 concentration of 21 mM, the stability and the homogeneity of the niosomal formulation declined, and increasing S60 concentration showed no effect on the mean particle size (Fig. 3). The observed results could be attributed to the formation of w/o/w vesicles from excess S60 moieties along with the stable DNP loaded niosomes. Fig. 4f shows the cryo-SEM images captured for NSV10 formulation containing 27 mM of S60 and 10 mM of CHOL. The findings exhibit the formation of other smaller vesicles along with the stable niosomes, despite purification of the formulation by mini-column centrifugation. The observations made were also ascertained by the HR-TEM image (Fig. 4a), which featured the formation of the spherical, bilayered, and hydrated vesicle when 10 mM of S60 was added to the PBS (pH 7.4). These translations proposed that the exclusion of these w/o/w vesicles from the formulation is indispensable to improve the stability and the homogeneity of the niosomal formulations.

Another possible explanation for the change in the mean particle size with variation in S60 concentration is based on critical packing parameter (CPP) which is given as the ratio of volume to the surface area as shown in Equation (5)

Critical Packing Parameter (CPP) = 
$$\frac{\theta}{a_0 l_c}$$
 (5)

Where  $a_0$  stands for the minimum interfacial area occupied by the hydrophilic head group,  $\upsilon$  is the lipophilic tail volume, and  $l_c$  is the lipophilic tail length.

CPP is a useful value as it allows the prediction of the molecular geometry of the aggregate complex formed by the monomers [57]. The predicted shape of the vesicle formed by S60 is spherical as the CPP value of the surfactant, S60, is between 0.5 and 1.0 [58]. Experimentally, the morphology of the vesicle system was observed by hydrating 10 mM of S60 in PBS at 65  $^{\circ}$ C, which corresponds to NCV1 formulation. The HR- TEM imaging revealed that the vesicles formed were spherical and bilayered (Fig. 4a).

However, the addition of other compatible lipophilic components into the formulation may alter the number of lipophilic groups, chain unsaturation, chain branching, and chain penetration affecting the parameter, v. The electrostatic interactions and head group hydration

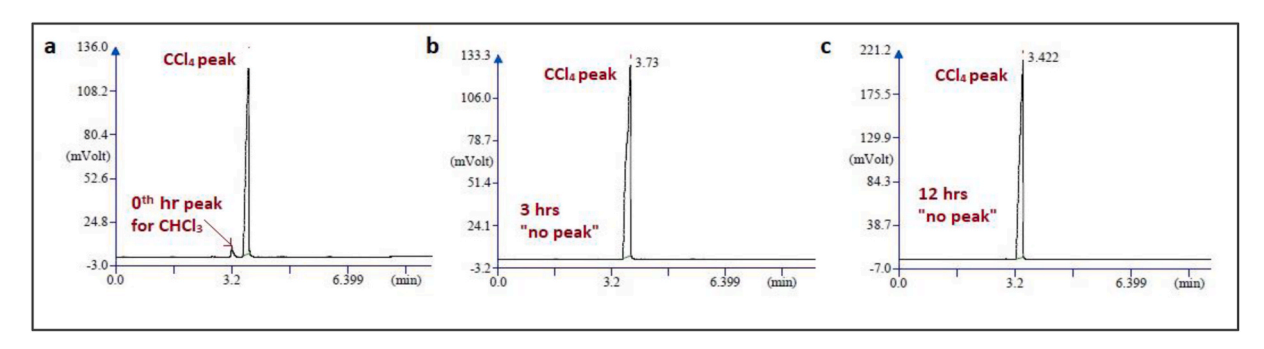


Fig. 2. Gas chromatogram of  $CHCl_3$  (retention time = 3.2min) and  $CCl_4$  (retention time = 3.6min). (a) Analyzed at  $0^{th}$  h of formation of the thin film. (b) 3 h of vacuum.

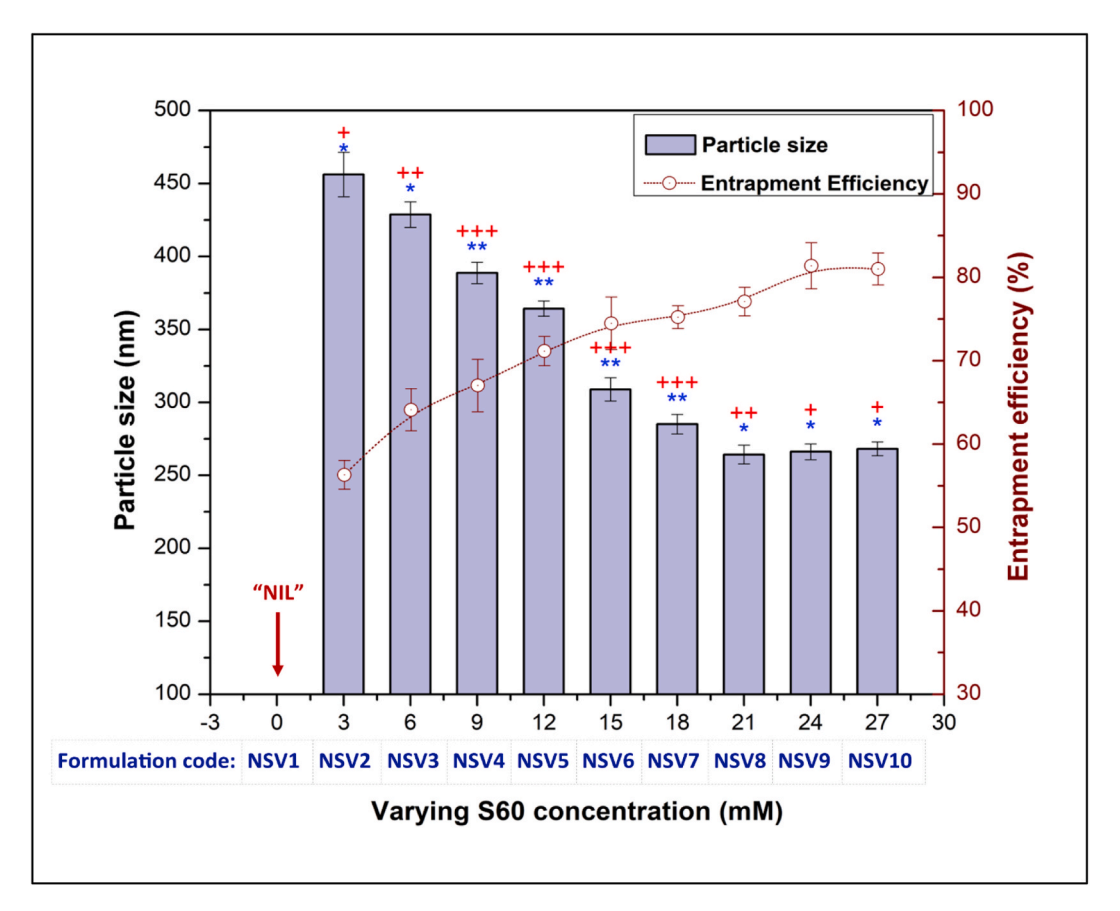


Fig. 3. Effect of S60 concentration on the mean particle size and entrapment efficiency.

Constant parameters: DNP loading:5 mg, CHOL concentration:10 mM, Hydration time:45 min, and Hydration Volume:10 ml.

Labels: \*\*\* PDI \le 0.2, \*\*\* PDI \le 0.5 and \*PDI \le 0.9. Degree of sedimentation observed on storage after 30 days at 4°C: +++ no sedimentation, ++ partial sedimentation (1–25%) and + near to complete sedimentation (1–70%).

may also modify the  $a_0$  value. The variations in these parameters can directly influence the CPP value and alter the morphology of the organized aggregate [59]. Although the mean particle size of the DNP niosomes decreased with an increase in the S60 concentration, the cryo-SEM images revealed that the conformation of the niosomes to be spherical, irrespective of the S60 concentration (Fig. 4). This structural elucidation implied that CPP value, even if altered, remained within the range of 0.5–1, thus forming spherical niosomes.

The investigation conclusively demonstrated that with the increase in S60 concentration, the mean particle size of the DNP niosomes scales down owing to the reduction in surface tension and stabilization on the niosome membranes. The results were in agreement with the findings reported by Essa (2010), where the niosome size reduced, irrespective of some differences in the surfactants used [51]. Similar results for S60 based spherical niosomes were reported by Khan et al. (2015) for diacerein, which exhibited a reduction in the mean particle size by 40% when S60 was increased by two times [60].

The effect of S60 concentration on entrapment efficiency was also investigated by varying the S60 molar concentration from 0 mM to 27 mM, and the results are represented in Fig. 3. The entrapment efficiency boosted significantly by 43.66% when S60 concentration was increased from 3 mM to 27 mM (p < 0.05). NSV9 formulation with 24 mM of S60 concentration registered an excellent entrapment of 81.62%  $\pm$  2.76%.

It is well accepted that water-insoluble drugs are preferentially taken up by the hydrophobic shell comprising of fatty acyl hydrocarbon chains, which provides an excellent solubilizing environment for the drug considered for the study. With the increase in S60 concentration, the volume of the hydrophobic domain increases, and the surface tension decreases, leading to the formation of smaller niosomes as well as

increase the niosomes count. Hence, the active surface available to accommodate the DNP too increases, resulting in higher entrapment efficiency. Similar results were reported by S60 niosomes of acetazolamide [61], carboxyfluorescein [56], and doxorubicin [30], indicating that lower the HLB value better is the entrapment efficiency. The findings may also be correlated to the hydrophobicity, alkyl chain length,  $T_{\rm c}$  of the S60, and the ordered gel state system of the bilayer shell formed in the niosome [62]. At a much higher concentration of S60, it can be contemplated that the S60 monomers may associate with themselves to form w/o/w vesicles entrapping the drug [63,64] along with the stable DNP niosomes, escalating the entrapment efficiency. Hence, it is crucial to eliminate the w/o/w vesicles formed for precise assessment of the entrapment efficiency of the stable DNP niosomes developed.

#### 3.3. Effect of CHOL concentration

CHOL is a lipid membrane additive that influences the shape, size, ion permeability, and elasticity of the niosomes [65]. The effect of CHOL on the physicochemical properties of the niosome was studied by synthesizing DNP loaded niosomes by varying CHOL concentration (0–27 mM), as shown in Fig. 5.

NCV1 formulation, with only S60 as the niosomal component, formed w/o/w vesicles (Fig. 4a) of 226.8  $\pm$  2.28 nm in the aqueous dispersion entrapping 28.73%  $\pm$  2.78% of DNP. From the data, it was observed that the mean particle size of the DNP niosomes reduced by 15.8% when CHOL concentration was varied from 3 mM to 12 mM (NCV2 to NCV5). A further rise in CHOL concentration till CHOL:27 mM, the mean particle size increased linearly by 38.4%. The formulation, NCV4, with a mean particle size of 288.71  $\pm$  2.1 nm and NCV5, with a

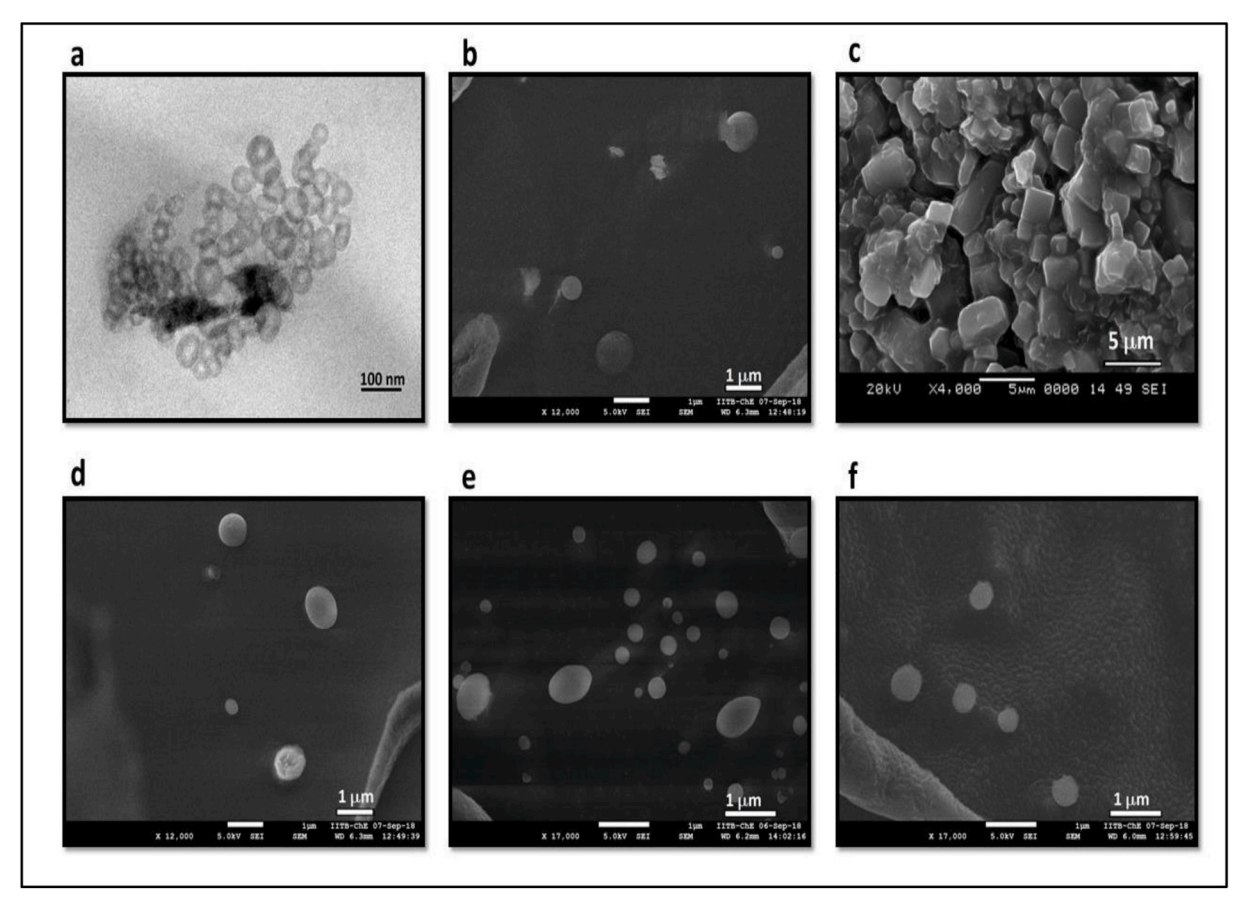


Fig. 4. (a) High-resolution TEM image of bilayer vesicles formed by hydrating 10 mM S60 in PBS, corresponds to NCV1 formulation. (b) Cryo-FEG-SEM image of NSV2 niosomal formulation (S60:3 mM: CHOL: 10 mM). (c) SEM image of Sediments of CHOL displaced from NSV2 niosomal formulation. (d) Cryo-FEG-SEM image of NSV5 niosomal formulation (S60:12 mM: CHOL: 10 mM). (e) Cryo-FEG-SEM image of NSV8 (S60:21 mM: CHOL: 10 mM) demonstrates non-homogeneity of the niosomal formulation. (f) Cryo-FEG-SEM image of NSV10 niosomal formulation (S60:27 mM: CHOL: 10 mM) vividly showcases the difference in the formation of stable niosomes along with w/o/w vesicles in the background.

mean particle size of  $288.3\pm5.73$  nm, demonstrated good homogeneity and stability. It was observed that the CHOL molecules behaved distinctively at varied concentrations. Therefore, understanding the mechanism by which CHOL incorporates in the bilayer is crucial to decipher the role of CHOL concentration in controlling the mean particle size of the DNP niosomes.

Being amphipathic, CHOL can incorporate itself into the bilayer membrane with its hydrophilic head oriented towards aqueous core and external phase while the aliphatic chain lines up parallel to the hydrocarbon chain in the center of the bilayer [66]. With the initial increase in the CHOL concentration, the CHOL molecules functioned as vesicular cement mortaring the cavities in the bilayer shell and strengthened the non-polar tail of the S60 monomers thereby, improving the chain order of the liquid state bilayer [24,66]. Hence, it is feasible to expect that the inclusion of optimum CHOL in the bilayer would result in close packing of S60 monomers, thus increasing curvature and reducing the mean particle size. However, at higher CHOL concentration, the gel state is transformed into a liquid order phase imparting disturbance in the architecture of the vesicular membrane, thus forming larger niosomes. The increase in the mean particle size may be ascribed to a dramatic alteration in the orientation order of the lipid hydrocarbon chains and associated thickening of the bilayer [67,68].

CHOL molecules are known to govern the membrane fluidity and elasticity by regulating the lipid organization and phase transition behavior. The four fused hydrocarbon ring in the steroid skeleton acts as a mortar in the membrane, thereby enhancing the entrapment efficiency and abolishes gel to sol transition [69]. It was observed that with the initial rise in CHOL concentration till CHOL: 9 mM, the entrapment

efficiency improved linearly. However, a further increase in CHOL concentration, above 9 mM, reduced entrapment efficiency by 44.5% (Fig. 5). The initial improvement in the entrapment efficiency with the increase in CHOL concentration may be attributed to the increase in hydrophobicity and stability of the niosomes formed [70] and a decrease in the permeability of the membrane [71].

In contrast, with further increase in CHOL concentration, the rigidity of the membrane increases, and the CHOL molecule may compete with the drug to orientate space within the bilayers, thereby excluding the drug from the vesicular membrane and reducing entrapment efficiency significantly [36,72]. The concentration of the CHOL molecule above the optimum concentration can disrupt the membrane and largely influence the entrapment efficiency [73]. Similar findings were reported for minoxidil niosomes [72], and colchicine niosomes [74], which demonstrated an initial increase in the entrapment efficiency followed by a reduction in entrapment efficiency upon the further increase in CHOL concentration. The reports suggested that a 1:1 M ratio of S60 and CHOL would be optimal to obtain the highest drug entrapment efficiency, which justifies our observation for NCV4 (S60:10 mM: CHOL: 9 mM) and NCV5 (S60:10 mM: CHOL:12 mM) formulations which demonstrated an excellent entrapment efficiency. The investigations revealed that fine-tuning CHOL concentration could significantly modify the entrapment efficiency of the DNP loaded niosomes.

## 3.4. Effect of sonication

Sonication is one of the most popular approaches applied to reduce the niosome size. Exposing the aqueous dispersion system to ultrasound

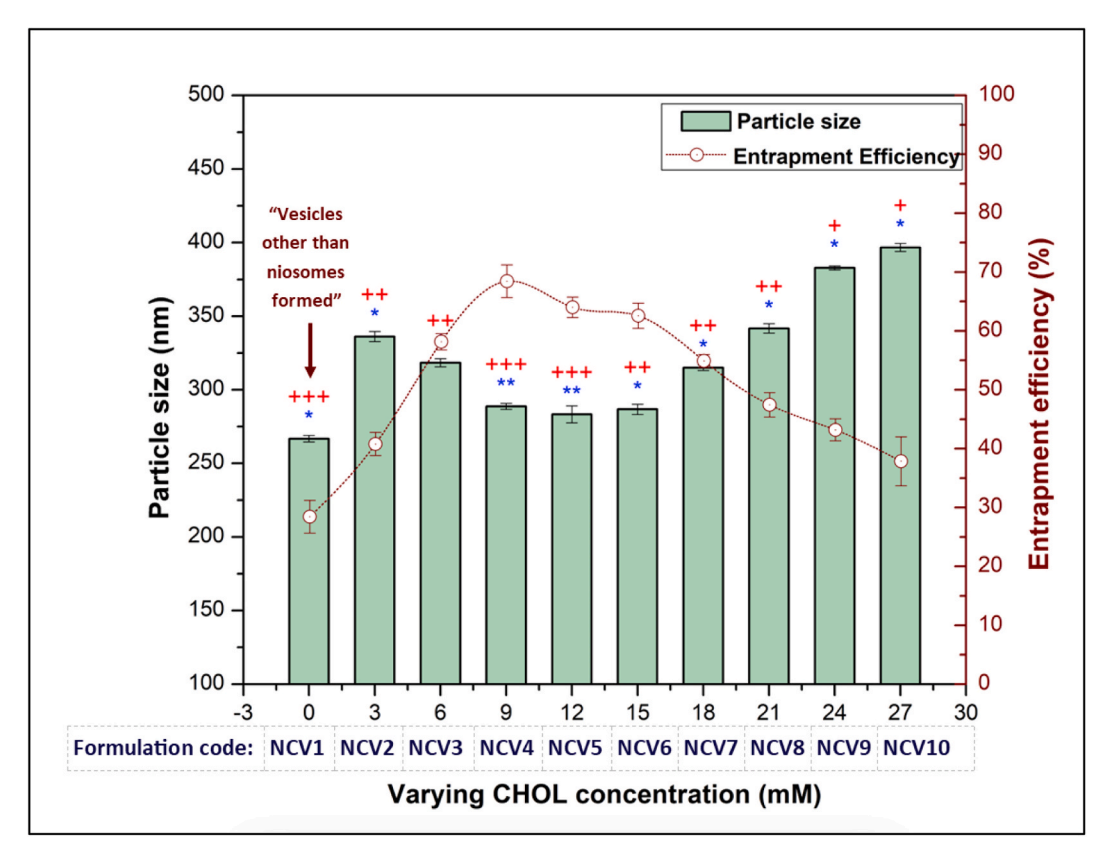


Fig. 5. Effect of CHOL concentration on the mean particle size and entrapment efficiency. Constant parameters: DNP loading:5 mg, S60 concentration:10 mM, Hydration Time:45 min, and Hydration Volume:10 ml.

<u>Labels:</u> \*\*\* PDI  $\leq$  0.2, \*\* PDI  $\leq$  0.5 and \*PDI  $\leq$  0.5 and \*PDI  $\leq$  0.9. Degree of sedimentation observed on storage after 30 days at 4 °C: +++ no sedimentation, ++ partial sedimentation (1–25%) and + near to complete sedimentation (1–70%).

generates cavitation, thereby altering the physical properties of the membrane to produce a homogenous population of niosomes [75]. However, sonication is a highly system-specific dispersion technique that involves concomitant complex physicochemical interactions that can result in either cluster breakdown or further agglomeration. Hence, in this investigation, we elucidate the effect of sonication to efficiently produce a homogenous population of DNP niosomes and its corresponding consequences on mean particle size and entrapment efficiency. The obtained results for probe sonicated DNP loaded niosomes were then compared with the non-sonicated niosomes.

#### 3.4.1. Effect of sonication on increasing S60 concentration

The effect of sonication on the physicochemical characteristics with increasing S60 concentration was assessed in conjunction with S60: CHOL ratio (Fig. 6). In comparison with the non-sonicated niosomal formulation, the probe sonicated formulations with the S60/CHOL ratio in the range of 0.9–2.7 demonstrated a superior effect on reducing the mean particle size of the DNP loaded niosomal formulations (NSV4-NSV10) while improving the homogeneity. The NSV4-NSV6 formulation exhibited a 30%–35% reduction in the mean particle size with narrow size distribution and registered an improvement in the PDI value and stability.

Analysis of the data in Fig. 6 reveals that S60 concentration and probe sonication influence the mean particle size of the DNP niosomes. The reduction in the mean particle size is attributed to the cavitation energy waves generated by the probe ultrasonicator. The cavitation energy produces vibrational shock waves to raise the pressure and shear stress due to which the membrane of larger niosomes breaks into smaller fragments, which folds up into thermodynamically stable niosomes of smaller size [76,77]. The cavitation energy also imparts high kinetic energy, which increases the collision frequency of the suspended

niosomes in the aqueous dispersion [78,79]. In principle, higher collision frequency enhances particle-particle impact event, which can perturb the bilayer organization leading to fragmentation or local increase in the curvature to form smaller niosomes. It can also result in the delamination of the outer shell by abrasion and erosion undergoing a transformation from larger multilamellar niosomes to small unilamellar niosome [76,80,81]. Conversely, probe sonication on NSV2 and NSV3 with S60/CHOL ratio of 0.3 and 0.6, exhibited a negligible effect on the reduction of mean particle size. The higher molar concentration of CHOL molecules in the niosomal formulation imparted membrane rigidity to subjugate the effect of sonication on reducing the mean particle size. The effect of sonication on increasing CHOL concentration is further discussed in Section 3.4.2.

In the context of entrapment efficiency, at S60/CHOL ratio of 0.3 (NSV2), entrapment efficiency reduced by 18.2%, while the S60/CHOL ratio from 0.6 to 1.2 showed no such deviations. The entrapment efficiency trendline diverged and established a continuing decline with a further increase in the S60/CHOL ratio. This gradual decline in the entrapment efficiency on sonication supported our conception of w/o/w vesicle formation at higher S60 concentration along with the stable niosomes, thus affecting the PDI and the stability. The probe sonication aided in the disruption of the w/o/w vesicle entrapping the drug fostering precise assessment of entrapment efficiency for the stable niosomes. Formulation NSV5 recorded a maximum entrapment efficiency of 73.3%  $\pm$  2.13% with a mean particle size of 240.3  $\pm$  2.738 nm to form a stable niosome.

It is well accepted that under the influence of probe sonication, for that S60-CHOL concentration, the larger bilayers may break up and upon self-assembly yield niosomes of smaller mean particle size [80,82,83]. The rapid re-equilibration of the S60 and CHOL molecules relieves the system of intra-bilayer tension and reduces the bending energy. As a

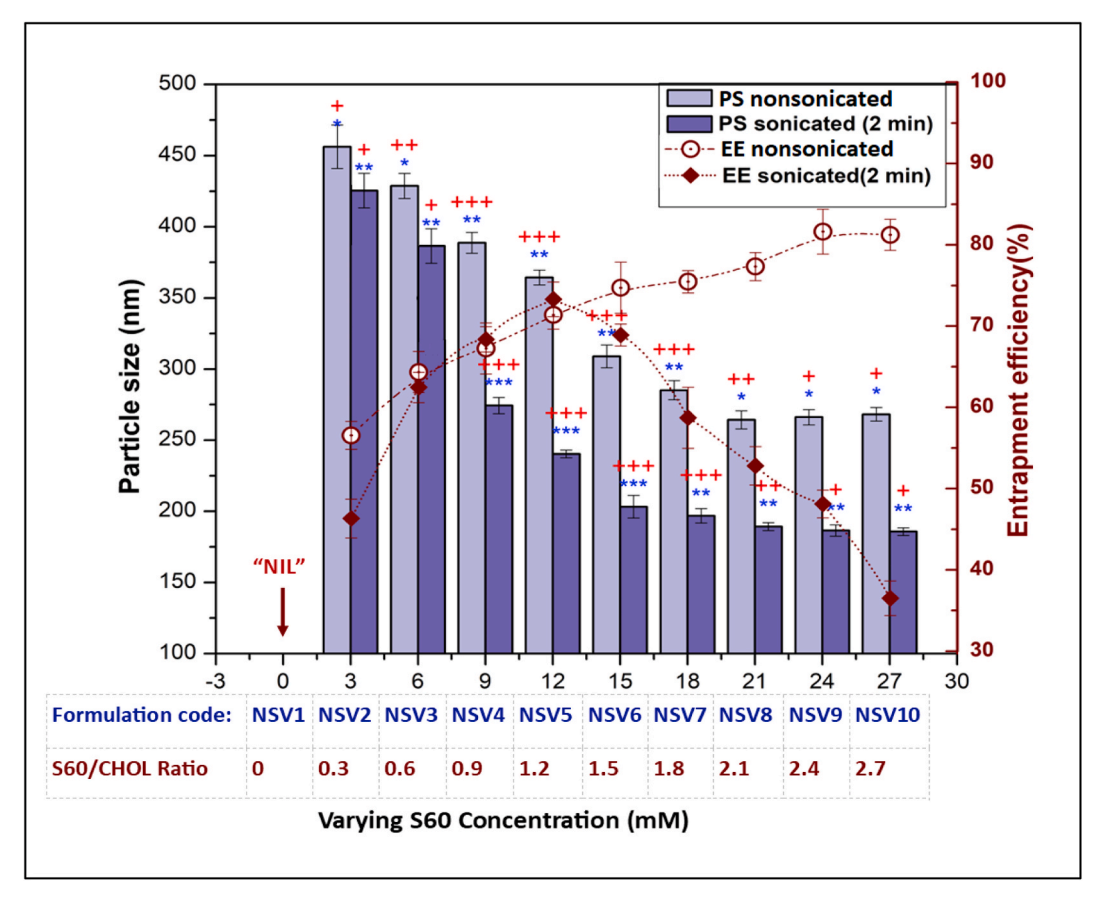


Fig. 6. Effect of sonication on varying S60 concentration

Constant parameters: DNP loading:5 mg, CHOL concentration:10 mM, Hydration Time:45 min, Hydration Volume:10 ml and sonication time: 2mins.

Labels: \*\*\* PDI value ≤ 0.2, \*\* PDI≤0.5 and \*PDI≤0.9. Degree of sedimentation observed on storage after 30 days at 4 °C: +++ no sedimentation, ++ partial sedimentation (1–25%) and + near to complete sedimentation (1–70%).

Abbreviations:: PS: mean particle size and EE: Entrapment efficiency.

consequence, thermodynamically stable vesicles are formed probably by flip-flop of S60 monomers to develop w/o/w vesicular system or form niosomes with an influx of CHOL molecules between the S60 molecules.

The chances of S60 monomer to form to w/o/w vesicular system or stable niosomes by incorporating the CHOL molecule largely depends upon S60 and CHOL concentration. Lasic (1995) postulated that at a higher level of S60 in the formulation, due to the asymmetric interactions across the bilayer, the monomers may detach from the bilayer and associate themselves to form w/o/w system by budding off mechanism [76]. The intrinsic ability of the S60 monomers, owing to its hydrophobicity coupled with hydrogen bonding and Van der Waals force, invokes the formation of w/o/w system. The vesicular system so formed also carries the ability to entrap DNP and hence are analog to DNP loaded niosomes. As a result, the entrapment efficiency for the DNP amplified with an increase in S60 concentration [84], as shown in Fig. 6.

As stated earlier, for the precise assessment of entrapment efficiency, it is vital to exclude the w/o/w vesicular system to improve the stability of the formulation. Hence, the formulation was subjected to sonication for 2 min. Sonication perturbs the bilayer organization of w/o/w vesicles resulting in fragmentation. And, in a temperature-controlled sonication system with temperature below the  $T_c$ , the inelastic bending prevents these small fragments from bending as the energy required to stretch/compress and fuse to form a vesicle is substantial [76]. The active surface areas available for drug entrapment dropped abruptly. As a consequence, the entrapment efficiency for DNP declined linearly with increasing S60 concentration beyond 12 mM. The percentage change in the entrapment efficiency between the sonicated and the non-sonicated formulation increased gradually with the increase in the S60/CHOL

ratio beyond 1.2, as shown in Fig. 6. Accordingly, probe sonication for 2 min, followed by mini-column centrifugation for purification of niosomal formulation, successfully demonstrated the removal of such vesicles formed and aided in precise evaluation of entrapment efficiency for DNP in the stable niosomes. The findings implied that the physicochemical properties of the synthesized niosome are accredited to the S60/CHOL ratio, as long as the amount of S60 is sufficient to amalgamate with the CHOL molecules to form stable niosomes.

## 3.4.2. Effect of sonication on increasing CHOL concentrations

CHOL molecules in niosomes are known to regulate the membrane elasticity and permeability. The effect of sonication on the physicochemical characteristics with increasing CHOL concentration was assessed in conjunction with S60: CHOL ratio (Fig. 7). The data shows erratic variations in the mean particle size distribution when compared to its corresponding non-sonicated formulations.

The analysis of data revealed that the effect of sonication on size reduction minimized with an increase in CHOL concentration. NCV1 formulation formed unstable vesicles (w/o/w system), which were reduced by 46.7% to produce smaller vesicles of 142.2  $\pm$  2.36 nm. For NCV4 (S60/CHOL ratio: 1.11) and NCV5 (S60/CHOL ratio: 0.83) formulations, the mean particle size diminished by 11% on sonication and displayed excellent stability and homogeneity (PDI $\leq$  0.2). The findings revealed that for every fraction of CHOL added, the effect of sonication on mean particle size reduced gradually. However, the impact of sonication on mean particle size was insignificant at higher CHOL concentration.

Generally, the larger niosomes are thought to be sheared into smaller

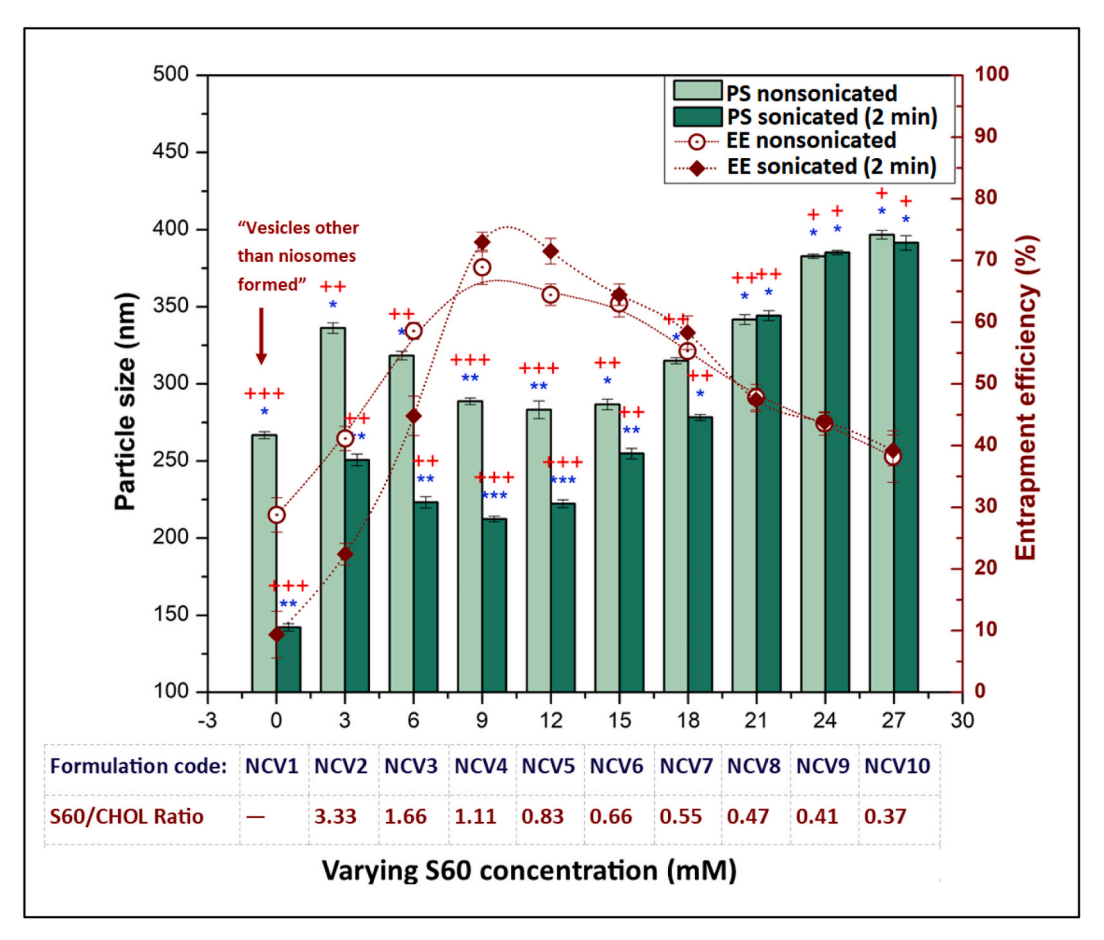


Fig. 7. Effect of sonication on vary CHOL concentration.

Constant parameters: DNP loading:5 mg, S60 concentration:10 mM, Hydration Time:45 min, Hydration Volume:10 ml and sonication time: 2mins.

Labels: \*\*\* PDI value ≤ 0.2, \*\* PDI ≤ 0.5 and \*PDI ≤ 0.9. Degree of sedimentation observed on storage after 30 days at 4°C: +++ no sedimentation, ++ partial sedimentation (1–25%) and + near to complete sedimentation (1–70%).

Abbreviations:: PS: mean particle size and EE: Entrapment efficiency.

ones under the influence of sonication due to their sensitivity to the applied frequency. Despite, subjecting the formulation to sonication, larger niosomes were formed contradicting our intuitive expectations. The data analysis ascertained that the effect of sonication on the mean particle size gradually reduced with an increase in CHOL concentration. At a low concentration of CHOL, the niosome membranes are more flexible and more liable to the effect of ultrasound waves, resulting in a smaller size. At CHOL concentration  $\geq$ 21 mM, sonication showed no effect on size reduction. The derived results could be explained based on the membrane rigidity resulting from CHOL inclusion. It is well established that the incorporation of CHOL diminishes the membrane flexibility and micro fluidity, which imparts physical stability to the niosomal systems [32,85].

Furthermore, it is known that CHOL increases the chain order of the liquid-state bilayer and strengthens the nonpolar tail of the surfactant [66]. The increase in the rigidity of the membrane offers resistance to sonication, thus showing no changes in the niosomal size at higher CHOL concentration. The increase in CHOL concentration can also dampen the cavitation process due to higher acoustic attenuation [79]. Hence it is recommended to synthesize niosomes with S60: CHOL ratio of 0.9–1.2 to form a homogenous population of stable niosomes.

From the perspective of entrapment efficiency for DNP, for the non-sonicated formulation NCV1, NCV2, and NCV3, the concentration of S60 was more than CHOL, which prompted for the formation of unstable vesicles along with the stable niosomes entrapping the DNP, the fact being validated by the poor PDI value and stability (as discussed earlier, Section 3.4.1). Sonication disrupted these unstable vesicles and

plummeted the entrapment efficiency by 67.5%, 45.6%, and 23.5% for NCV1, NCV2, and NCV3, respectively. For S60: CHOL ratio of 1.11 and 0.83, sonication boosted entrapment efficiency by 6% and 11% distinctively. Further increase in CHOL concentration converged the entrapment efficiency trendline of sonicated and non-sonicated formulation and exhibited a negligible effect on entrapment efficiency owing to the membrane rigidity conferred by the increased CHOL concentration. Such an influx of the CHOL molecules can displace the drug from the niosome shell adversely, effecting the entrapment efficiency. Of all, NCV4 exhibited excellent entrapment efficiency of  $72.84\% \pm 1.56\%$  with the mean particle size of  $212.37 \pm 1.76$  nm and hence considered for further optimization.

In all, it brought to view that the S60: CHOL ratio is of utmost importance, which has to be operated within the design space for the formulation of stable niosomes of optimum size and excellent entrapment efficiency. The investigations revealed that the energy input by sonication and S60/CHOL ratio, which determines the bending elasticity and mechanical cohesivity of the niosomal shell, steers the physicochemical characteristic of the DNP loaded niosomes. Based on the stability, PDI, mean particle size and entrapment efficiency, NSV5 (S60/CHOL ratio: 1.2) and NCV4 (S60/CHOL ratio: 0.83) formulation was considered for further investigations.

#### 3.5. Effect of hydration volume

Hydration volume and hydration time are also the critical parameters that define the shape and size of the niosomes. Improper selection of

these parameters may result in the formation of fragile and leaky niosomes. The hydration time was fixed at 45 min as the uniformity of niosome shape depends on hydration time [86]. Four groups of formulation were considered for the study viz., blank niosomes of NSV5, DNP loaded niosomes of NSV5, blank niosomes of NCV5, and DNP loaded niosomes of NCV4, to understand the effect of hydration volume on the physicochemical characteristics of the niosomes. The hydration volume was varied from 2.5 to 30 ml, while the drug loading (5 mg), hydration time (45 min), and probe sonication time (2 min) were kept constant.

Analysis of the data revealed that at the hydration volume of 2.5 ml, larger niosomes were formed with relatively low entrapment efficiency, as shown in Fig. 8a and b. The particle size analyzer recorded a mean particle size of 288.7  $\pm$  7.36 nm and 275.3  $\pm$  5.78 nm for DNP loaded niosomes of NSV5 and NCV4, respectively. The formulations were unstable, and drug precipitated within 6 h of annealing time. From the

result, it appears that low hydration volume hinders the association of the S60 and CHOL to form stable niosome. Also, low hydration affects the hydrophilic head area ( $a_o$ ) value adversely, leading to the increase CPP value and formation of niosomes of non-uniform shape and size, which primarily affects the PDI and stability of the formulation.

With the increase in hydration volume above 5 ml, the mean particle size of DNP loaded niosomes of NCV4 and NSV5 increased (p < 0.05). From the preliminary studies, it appears that with the increase in hydration volume, either the water molecules intercalated between the bilayer in the shell increasing the hydrodynamic diameter of the niosome or it is likely to restructure the bilayers to form the multilamellar niosome. Presuming that multilamellar niosomes are developed, then the entrapment efficiency of the niosomes is bound to increase as the drug preferentially partitions into the multi-bilayer of the niosomes, thereby increasing the surface area available for drug incorporation. On

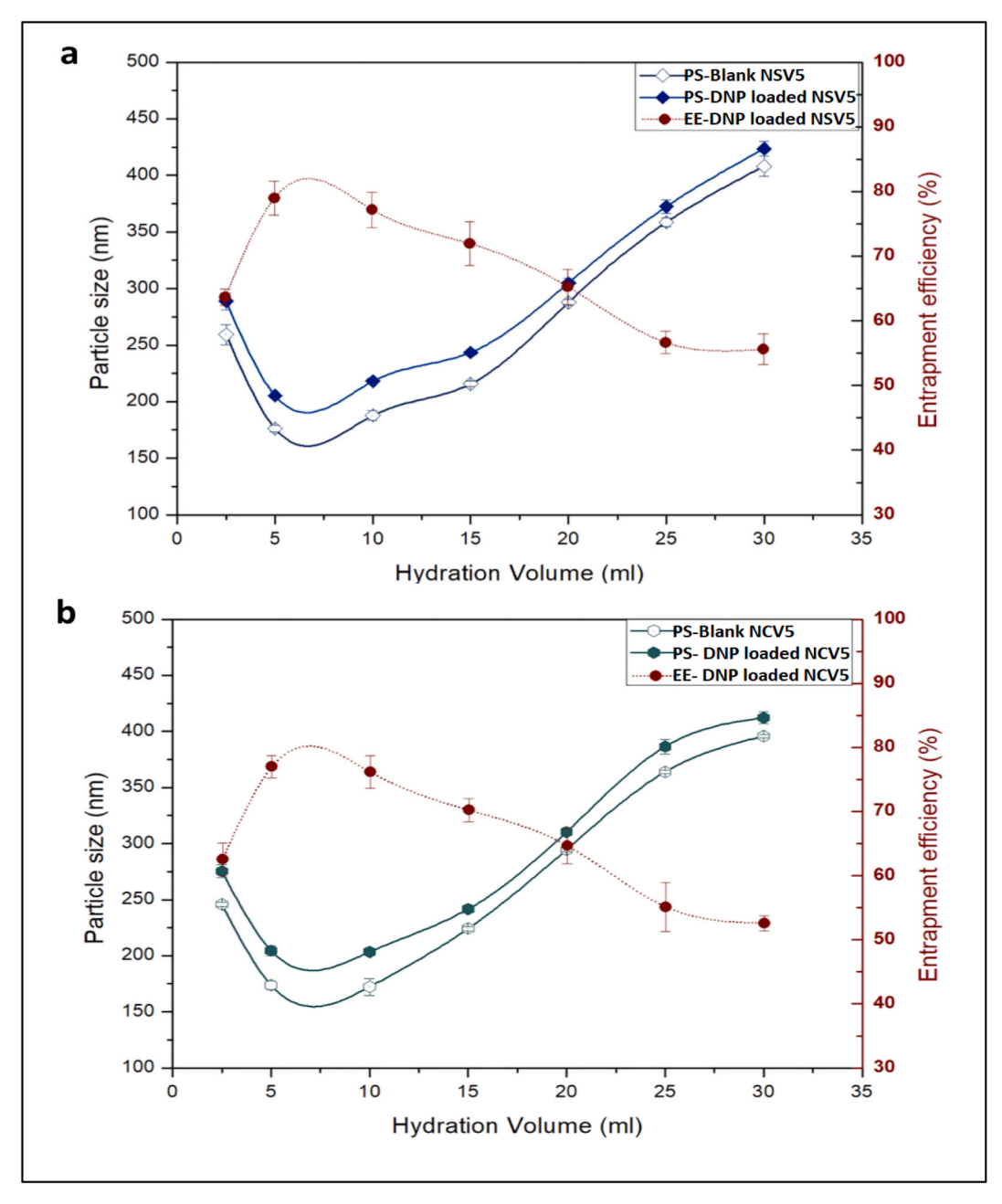


Fig. 8. (a) Effect of hydration volume on the mean particle size and entrapment efficiency of NSV5-loaded and NSV5-Blank. (b) Effect of hydration volume on mean particle size and entrapment efficiency of NCV4-loaded and NCV4-Blank.

Abbreviations:: PS: Mean particle size and EE: Entrapment efficiency.

the contrary, DNP loaded niosomes of NSV5 and NCV4 displayed a significant reduction in the entrapment efficiency (p < 0.05) with the increase in hydration volume. Hence, the theory of water inclusion theory in the membrane is proposed.

To further validate, blank niosomes for NSV5 and NCV4 were synthesized, and its mean particle size was compared with its corresponding DNP loaded niosomes. Analysis of the data in Fig. 8 shows that the mean particle size of the DNP loaded niosomes increased linearly from 205.22  $\pm$  3.8 nm to 423.7  $\pm$  2.78 nm for NSV5 and 204.5  $\pm$  5.34 nm to 412.34  $\pm$  3.28 nm for NCV4 with an increase in the PDI. Essa (2000) postulated the drug inclusion theory into the membrane, suggesting that the drug partitions into the membrane, increasing the hydrodynamic diameter by approximately 30% [51]. On that account, with the increase in the hydration volume, the DNP concentration should reduce. And hence, the DNP molecule available for accommodating into the shell is narrowed.

As a consequence, the bulkiness of the niosome shell should have been contracted, producing niosomes of smaller size. On the contrary, the mean size of the DNP loaded niosomes increased despite the reduction in entrapment efficiency. Similar trends were observed for the blank niosomes of NSV5 and NCV4, which ascertained our hypothesis that the water molecule intercalates between the membrane by replacing the drug and lead to the swelling of the lipid layer to form entropically stable hydrated niosomes. The results were in agreement with the investigations carried out by Claessens et al. to study the effect of ionic strength on the membrane rigidity, size, and the stability of the lipid vesicles who reported that negatively charged niosomes of phospholipids continuously swell in pure water [87].

At a hydration volume of 5 ml, entrapment efficiency of 79.13%  $\pm$  2.63% (NSV5) and 77.15%  $\pm$  2.14% (NCV4) was recorded, which explains the fact that optimum DNP concentration is achieved in the bilayer shell of the niosomes. Further increase in the hydration volume diluted the drug concentration in the suspension and incorporated the water molecule in the bilayer, thus reducing the EE proportionately. Ruckmani and Sankar reported that the increase in the hydration volume formed leaky niosomes [36]. Similar results were reported for ketorolac liposomes [88], confirming that entrapment efficiency decreases with the increase in hydration volume.

Of the two, NSV5 formulation loaded with 5 mg of DNP hydrated in 5 ml of PBS for 45 min recorded a good entrapment efficiency of 79.13%  $\pm~2.63\%$  and a mean particle size of 205.4  $\pm~2.7$  nm, and hence considered for further studies.

## 3.6. Effect of membrane additives and stability studies

Theoretically, niosomes require of a particular class of amphiphile to prevent aggregation. Therefore, a membrane additive is often included in the formulation to alter the biodistribution or to improve the stability of the formulation via electrostatic means or stearic stabilization. Bilayer membrane additives are lipid excipients or edge activators which are incapable of forming surfactant vesicle on their own but can be integrated into the bilayer shell. Hence, to study the effect of

membrane additives on the characteristic of the niosomes, commonly used DCP and SolC24 was considered for the study. The chemical structure of the DCP and SolC24 is given in Fig. 9. DCP, an anionic surfactant, is known to enhance the stability of the formulation [36,89, 90] while SolC24, a non-ionic molecule, is known to enhance the biodistribution of the niosomes in brain tissue [30,91–94]. The concentration of the edge activator was selected based on our preliminary studies. The data is included in supporting information (Fig. S3).

The permissible limit of 10 mM of SolC24 was suggested by Marco Bragagni et al. (2012) based on the cytotoxicity studies while Arunothayanun et al. (2000) proposed the addition of 10% SolC24 to the formulation [29,30]. Hence, experiments were conducted to study the effect of SolC24 concentration by varying the concentration from 1 to 10 mM. Considering the parameters such as optimum niosome size and entrapment efficiency, the SolC24 concentration was fixed to 5 mM. Hence, 5 mM of the edge activator, Sol C24, was added individually into the optimized NSV5 formulation to get NSV5<sub>SolC24</sub>. Similarly, 5 mM of DCP was added to NSV5 formulation to form NSV5<sub>DCP</sub> niosomes. Comparative studies for the variation in its physicochemical properties are presented in Table 2 and Fig. 10.

Analysis of the data revealed that the inclusion of membrane additives into the NSV5 formulation influences the mean particle size. Finding demonstrated an 18.7% increase in the mean particle size of NSV5<sub>DCP</sub>, while the mean particle size of NSV5<sub>SolC24</sub> reduced by 12.2% when compared to that of NSV5 formulation. Of the three, the NSV5<sub>SolC24</sub> formulation demonstrated a higher degree of homogeneity with a PDI value of 0.12 and a mean particle size of 180.1  $\pm$  1.83 nm. In comparison, NSV5<sub>DCP</sub> formed larger niosomes with a mean particle size of 243.8  $\pm$  2.76 nm.

The increase in the mean particle size of the NSV5 $_{DCP}$  niosomes can be explained based on a different mechanism. Firstly, the assimilation of DCP into the bilayer can build up the volume of aqueous compartment between the adjacent bilayer membrane in multilamellar niosomes by charge repulsion and induce the formation of larger NSV5 $_{DCP}$  niosomes [95,96]. Secondly, the interplay between the two cetyl chain of DCP and

**Table 2**Physicochemical characterization of the niosomal formulations to study the effect of membrane additives.

Formulations code	Mean Particle Size (nm)	PDI	Zeta- potential (mV)	Entrapment efficiency (%)
NSV5	$205.4\pm2.7$	0.19 ± 0.046	$-24.7 \pm 3.16$	$79.13 \pm 2.63$
NSV5 <sub>DCP</sub>	$\textbf{243.8} \pm \textbf{2.76}$	$\begin{array}{c} 0.315 \; \pm \\ 0.041 \end{array}$	$-40.9 \pm 2.73$	$61.62\pm1.73$
NSV5 <sub>Sol C24</sub>	$180.1\pm1.83$	$\begin{array}{c} 0.12 \pm \\ 0.007 \end{array}$	$-32.7 \pm \\1.17$	$82.15\pm1.54$

The data reported is an average of 3 measurements (mean  $\pm$  SD). Formulations stored at 4  $^{\circ}C$  and the measurement were carried out after 24 h of synthesis.

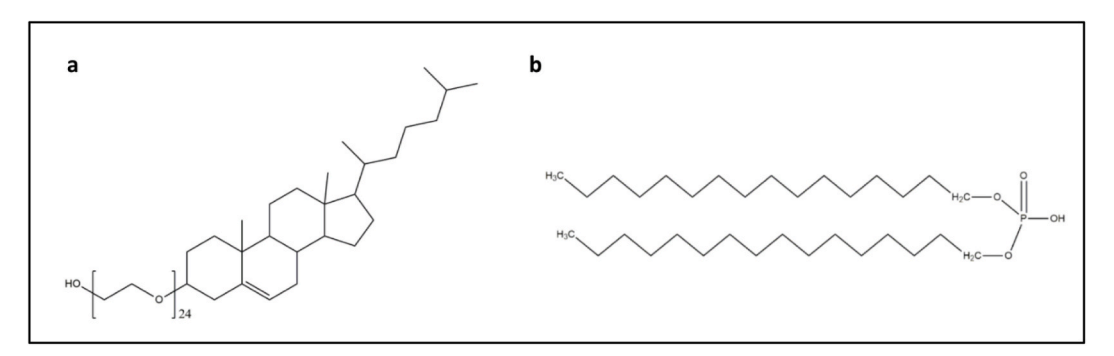


Fig. 9. Chemical structure of (a) SolC24 (Mol.Wt:1442.71) (b) DCP (Mol.Wt:546.48).

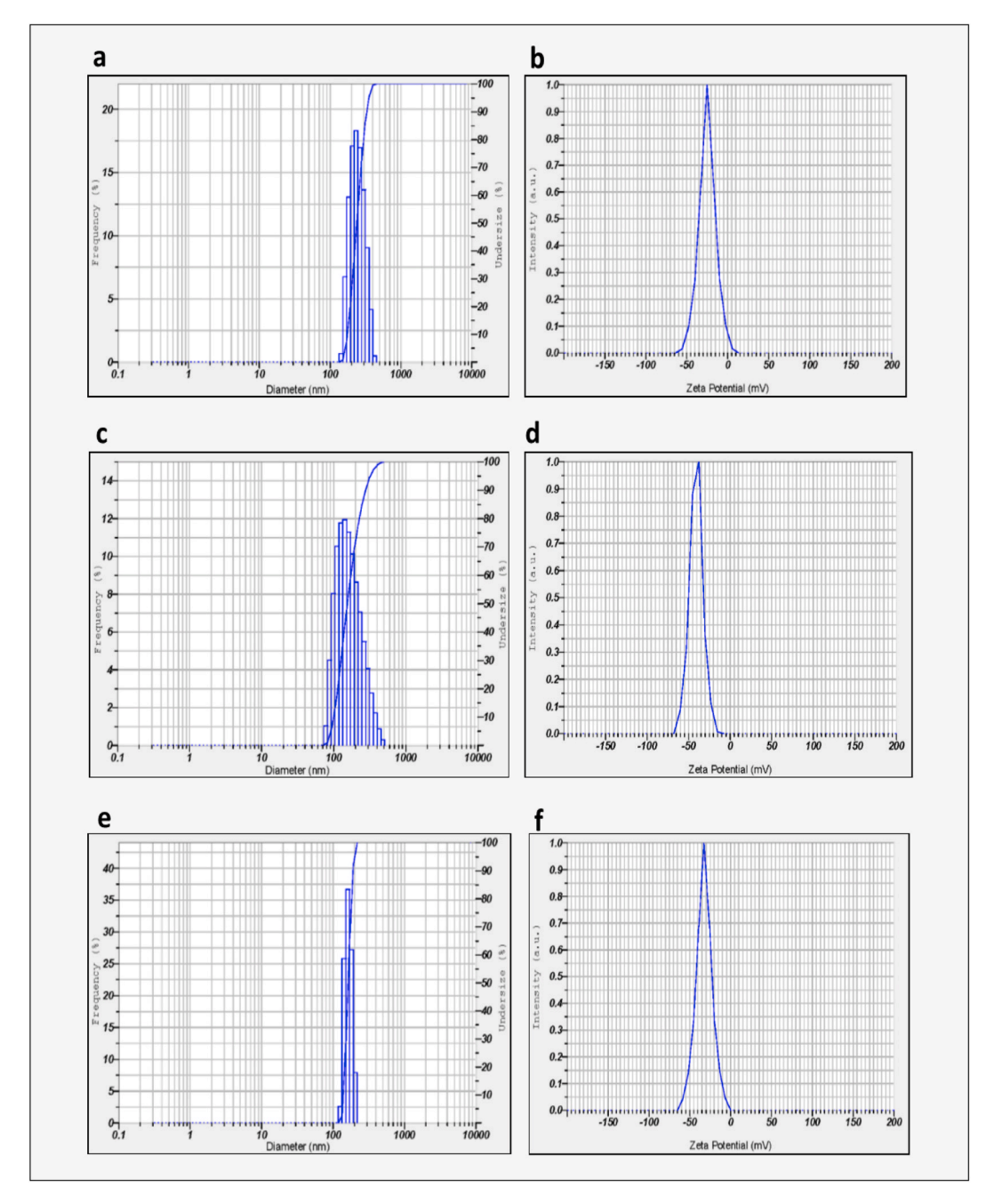


Fig. 10. (a) Size distribution of NSV5 formulation (b) Zeta potential of NSV5 formulation (c) Size distribution of NSV5<sub>DCP</sub> formulation (d) Zeta potential of NSV5<sub>DCP</sub> formulation (e) Size distribution of NSV5<sub>Sol C24</sub> formulation (f) Zeta potential of NSV5<sub>SolC24</sub> formulation.

stearyl chain of S60 reduces the ability of the surfactant to curve and split, which might result in less tightly packed bilayer membranes producing larger NSV5 $_{\rm DCP}$  niosomes [96–98]. Another possible interpretation could be the inclusion of DCP molecules into bilayer could have led to mutual repulsion between the charged moiety and the S60 head groups, thereby increasing the hydrodynamic diameter of the niosome [51,99].

Intriguingly, the addition of SolC24 into the formulation decreased the mean particle size despite its massive structure, as compared to NSV5 formulation. Similar findings were reported by Junyaprasert et al. (2008), who demonstrated that the inclusion of SolC24 into the niosomes could reduce the mean particle size [89]. The reduction in the NSV5 $_{\rm SolC24}$  can be attributed to its hydrophobicity of SolC24. The decline in the mean particle size of NSV5 $_{\rm SolC24}$  can be elucidated based on SolC24 positioning within the bilayer, as proposed by Abdelkader

et al. (2011). The hypothesis states that the SolC24 molecule embeds between the aliphatic stearyl chains of S60 molecule within the bilayer resulting in a tightly packed bilayer due to the strong interactions of Sol C24 with S60 and CHOL. While the two-chained DCP molecule which traverses through the breadth of the bilayer with the -HPO4 head group facing the aqueous phase producing larger NSV5 $_{\rm DCP}$  niosome [99,100]. The results revealed that the nature and structure of membrane additives could critically influence the membrane fluidity, rate of curving, and splitting of the bilayer membrane, which in turn regulates the mean particle size.

The significance of the zeta potential is that its values can be correlated to the electrophoretic movement of the particles and stability of the formulation. The zeta potential value of NSV5, NSV5 $_{DCP}$ , and NSV5 $_{SolC24}$  are presented in Table 2 and Fig. 10 (b, d, and f). Despite S60 being non-ionic, the NSV5 formulation registered a negative charge of

 $-24.7\pm3.16$  mV, which can be ascribed to the preferential adsorption of counterions or the hydroxyl ions on the niosome shell.

Inclusion of DCP, increased the charge density of the bilayer membranes in NSV5<sub>DCP</sub> due to ionization of the acidic (-HPO<sub>4</sub>) as reflected by the high zeta potential value of  $-40.9\pm2.73$  mV. Similar studies were reported for zidovudine niosomes [36],  $\beta$ -estradiol niosomes [51], and salicylic acid niosome [89], which implied that the formulations were stabilized by electrostatic repulsion. With regard to SolC24, despite being a non-ionic molecule, the zeta potential of NSV5\_Solc24 improved by 32.4%. The improvement in the zeta-potential is attributed to the entropic stabilization of the long hydrophilic polyoxyethylene chain of SolC24 and a shift in the shear plane, which hinders the association of vesicles [32,89]. The improved electrophoretic mobility of the particles confers it with a stearic shield, which prevents the particle from aggregation, thus improving the stability of the NSV5<sub>SolC24</sub>.

Concerning the entrapment efficiency, NSV5<sub>DCP</sub> exhibited a

reduction in the entrapment efficiency by 22.13%, while NSV5<sub>SolC24</sub> showed a nominal increase in entrapment efficiency by 3.82% (Table 2). The possible explanation for low entrapment efficiency in NSV5<sub>DCP</sub> can be ascribed to the electrostatic repulsion force between the DCP, S60, and CHOL head groups within the bilayer membrane, which squeezes out the drug from the membrane, thereby reducing the entrapment efficiency [56,72,101]. However, NSV5<sub>DCP</sub> was stable over three months of storage with approx. — 7% of the DNP leaching out. On the other hand, NSV5<sub>SolC24</sub> exhibited a negligible effect on entrapment efficiency and recorded an entrapment efficiency of 82.15%  $\pm$  1.54%. The NSV5<sub>SolC24</sub> formulation was stable over six months with approx. — 3% leaching out of the drug. The higher entrapment efficiency may be attributed to the affinity of the SolC24 molecule to associate with S60 and CHOL reducing the membrane permeability and elasticity, consequently retaining more drugs. Similar results were reported for niosomes bearing transferring and glucose ligand [102] and vasoactive intestinal

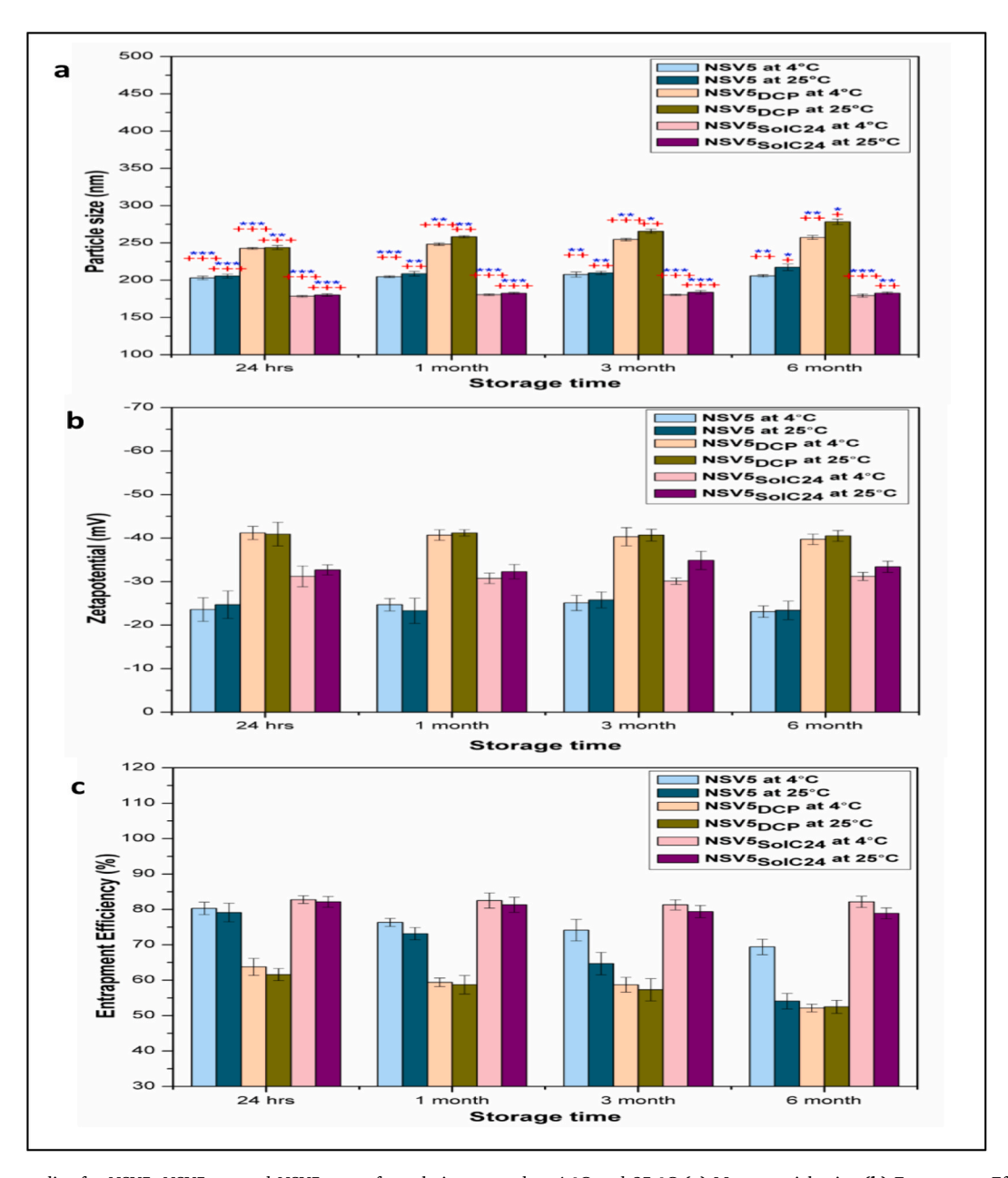


Fig. 11. Stability studies for NSV5, NSV5<sub>DCP</sub>, and NSV5<sub>Sol C24</sub> formulations stored at 4  $^{\circ}$ C and 25  $^{\circ}$ C (a) Mean particle size (b) Entrapment Efficiency (c) Zeta potential.

Labels: \*\*\* PDI value  $\leq 0.2$ , \*\* PDI $\leq 0.5$  and \*PDI $\leq 0.9$ . Degree of sedimentation observed on storage after 30 days at 4°C: +++ no sedimentation, ++ partial sedimentation (1–25%) and + near to complete sedimentation (1–70%).

peptide-loaded niosomes [93] and doxorubicin niosomes [30].

#### 3.7. Stability studies

During storage, swelling of the membrane bilayer, drug leakage, and loss in the number of vesicles can alter the physicochemical characteristics of the niosome and influence the stability of the formulation. Niosomes are self assembles of S60, CHOL, and membrane additives entrapping drug into closed bilayers structures. However, hydrated niosomes are not considered to be thermodynamically stable and can undergo chemical degradation, such as oxidation and hydrolysis, to form leaky niosomes. The electrophoretic mobility conferred to the niosomes can also lead to the fusion of the niosomes to form aggregates during storage.

Hence, the long-term stability of all the formulations was assessed for its transition in the physicochemical properties. The formulation, NSV5 $_{\rm DCP}$ , and NSV5 $_{\rm SolC24}$  were stored at 4  $^{\circ}$ C and 25  $^{\circ}$ C and samples were withdrawn after a period of one, three, and six months to evaluate mean particle size, PDI, zeta potential, and entrapment efficiency as shown in Fig. 11. The degree of sedimentation of the prepared formulations was recorded based on its physical appearance.

The analysis of the data (Fig. 11a) revealed that the mean particle size of the NSV5<sub>DCP</sub> increased by 13.2% (stored at 25 °C) and 6.02% (stored at 4 °C) over six months of storage. The entrapment efficiency of the formulation too reduced by 31.2% when stored at 25 °C and by 13.6% when stored at 4 °C over a storage time of 6 months. The increase in the mean particle size and reduction in the entrapment efficiency is attributed to charge repulsion, as mentioned previously. The NSV5 formulation stored at 25 °C showed a 5.8% increase in the mean particle size, while storage at 4 °C displayed a negligible effect. However, the entrapment efficiency reduced irrespective of storage temperatures. Similar results were observed concerning the degree of sedimentation and homogeneity. Both NSV5<sub>DCP</sub> and NSV5 registered near to complete sedimentation and inferior PDI value.

In comparison, NSV5 $_{SolC24}$  showed a negligible effect on the mean particle size, zeta-potential, entrapment efficiency, or the homogeneity irrespective of the storage temperature or storage duration. The observed effect can be attributed to the steric stabilization endowed by the SolC24 molecules lowering the prospect of niosome aggregation. Additionally, the  $T_c$  of SolC24 is 50 °C [99] and hence exist in the gel phase at a lower temperature after hydration. The gel phase of SolC24, coupled with S60 and membrane-stabilizing effect of CHOL, binds the drug molecules together and prevents drug leakage. Also, NSV5 $_{SolC24}$  formulation showed good PDI value < 0.2 and no signs of sedimentation despite extended storage time.

# 3.8. Release kinetic studies for DNP from NSV5 $_{SolC24}$ at different physiological pH

Niosomal formulation, NSV5 $_{SolC24}$  with a DNP loading of 5 mg, was subjected to *in vitro* release studies at pH 5.4 (topical skin), pH 6.8 (brain), and pH 7.4 (blood plasma) to evaluate its response to pH variations. From the data obtained, it was observed that at pH 7.4, the drug release lasted till 105 h, with 95.7%  $\pm$  0.986% of the entrapped DNP being released. At pH 6.8 simulating the brain, the NSV5 $_{SolC24}$  demonstrated sustain release profile with 98.17%  $\pm$  1.65% of the drug being

released over 6 h. While at pH 5.4, burst release was observed, and  $98.17\% \pm 1.65\%$  of the drug was released within 3 h. The results reflected the pH sensitivity of NSV5<sub>SolC24</sub>.

In an attempt to understand the drug release mechanism at different pH, the *in vitro* release studies data were fitted into the kinetic model. The correlation coefficients for zero order, first order, Higuchi matrix, Hixson-Crowell, and Korsmeyer-Peppas equation were calculated (Table 3). The Fickian diffusion mechanism best expressed overall curve fitting for DNP release from the NSV5<sub>SolC24</sub>formulations at pH 7.4 and pH 5.4.

At pH 7.4, the DNP release for the formulation fitted in a zero-order model, releasing 0.953% of the drug/h with high linearity and  $r^2=0.991.$  While the formulation at pH 5.4, followed the first-order model with  $r^2=0.969$  with initial burst release of the drug. At pH 6.8, the release kinetics fitted well in the Korsmeyer-Peppas model with release exponent, n=1.35, and corresponded to non-fickian diffusion with super case-II anomalous transport/relaxation [103]. At pH 5.4 simulating the topical skin, the 92.59%  $\pm\,1.311\%$  of DNP was released within 3 h, which implies that NSV5\_SolC24 can be effectively used for topical treatment such as allergy, burns, wounds, and skin cancer. However, embedding the formulation into a MN system could bypass the pH barrier and stratum cornea of the skin to facilitate transdermal delivery of intact NSV5\_SolC24 into the systemic circulation, thereby aid in the controlled and sustained release of DNP at the target site.

#### 3.9. Evaluation of pH sensitivity

The surface morphological changes of NSV5 $_{SolC24}$  induced by pH change were evidenced by cryo-SEM imaging in Fig. 12. To further validate the structural change in the NSV5 $_{SolC24}$  niosomes, FTIR spectral peaks of the functional groups were recorded for the niosomes at different pH, as shown in Fig. 13.

At pH 7.4, FTIR spectra for blank niosomes of NSV5<sub>SolC24</sub> showed characteristic peaks for -OH broad spectra at 3471.49 cm<sup>-1</sup>, strong asymmetric stretching of aliphatic -CH at 2922.82 cm<sup>-1</sup> and 2854.39 cm<sup>-1</sup>, in-plane bending vibration of C=O at 1737.78 cm<sup>-1</sup> and rocking vibration of -O-CH<sub>2</sub> at 1643.96 cm<sup>-1</sup> corresponded to the ester group of S60. Deformation vibration at 1464.47 cm<sup>-1</sup> corresponded to C=C while bending at 1344.46 cm<sup>-1</sup> corresponded to O-CH of the tetrahydrofuran of S60. Out of plane bend at 1280.90 cm<sup>-1</sup> and 1244.2 cm<sup>-1</sup> was registered for -CH of alcohol groups. Furthermore, out of plane angular deformation vibrations for C-H was noted at 948.44 cm<sup>-1</sup> and  $845.43 \text{ cm}^{-1}$  [104,106]. The interplay between the glycerol oxygen of S60 and  $\beta$ -OH of the CHOL is the basis for membrane stabilization in the niosome membrane [106,107]. The sharp stretching peak for the ether group of Sol C24 was recorded at 1092.48 cm<sup>-1</sup>, indicating the compatibility of SolC24 with other excipients and its successful assimilation into the membrane bilayer. The niosome, NSV5<sub>SolC24</sub> formed were spherical, as demonstrated by the cryo-SEM imager.

At pH 6.8, a protruding peak was registered at 3359.31 cm<sup>-1</sup> for alkane attached alcohol within the broad spectrum of the hydroxyl group. There was a shift of ester peak from 1737.78 cm<sup>-1</sup> to 1709.19 cm<sup>-1</sup>, which corresponds to C=O weak stretching vibration of saturated carboxylic acid. The transition in the peak may be attributed to the acid hydrolysis of the ester molecule of S60 to form diols and carboxylic acid. A diol is a compound containing two hydroxyl groups reflected by its

**Table 3**Determination of the order of DNP release from NSV5<sub>SolC24</sub>.

	Zero-ord	er	First-ord	er	Higuchi		Hixson-C	rowell	Korsmey	er Peppas	Release mechanism
	$r^2$	K <sub>0</sub> % mg/h	r <sup>2</sup>	$K_1 h^{-1}$	$r^2$	K <sub>H</sub>	$r^2$	K%mg/h	$r^2$	n	
Plasma pH 7.4	0.991	0.953	0.925	0.026	0.882	8.17	0.883	0.029	0.412	NA	FD
Brain pH 6.8	0.985	16.36	0.845	0.586	0.941	36.53	0.946	0.486	0.996	1.35	NFD Supercase-II
Skin pH 5.4	0.774	28.21	0.969	0.829	0.949	58.53	0.875	1.006	0.959	1.85	FD

Abbreviations: NA= Not Applicable, FD= Fickian Diffusion, NFD=Non Fickian Diffusion.

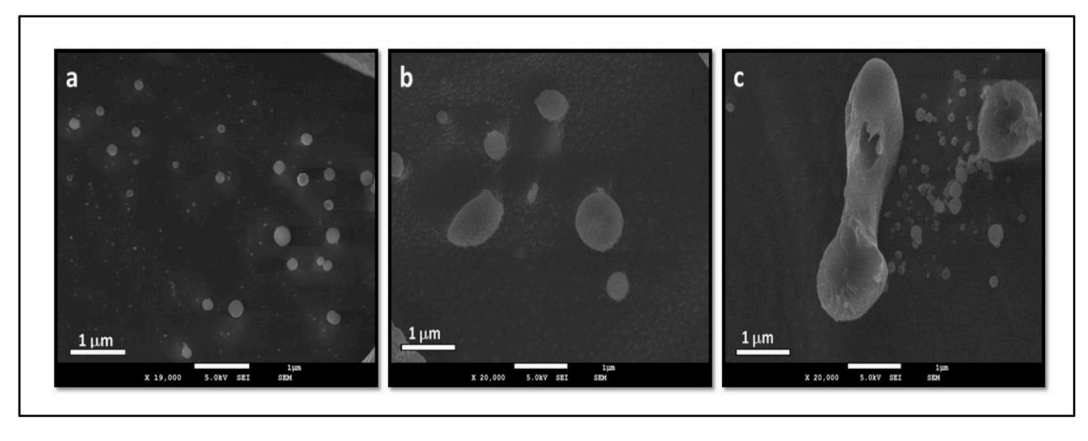


**Fig. 12.** Comparative cryo-SEM image of hydrated NSV5<sub>SolC24</sub> at different physiological pH. (a) At pH 7.4 simulating blood plasma (b) At pH 6.8 corresponding to AD brain (c) At pH 5.4 simulating skin.

corresponding two peaks in the range of 3000 cm<sup>-1</sup> to 3500 cm<sup>-1</sup> [108]. The observed spectral peak at 1344.46 cm<sup>-1</sup>, which corresponds to the O–CH of the tetrahydrofuran of S60, showed no deviations. The finds suggested that the 5-membered cyclic ring of the S60 was structurally intact and did not undergo any cyclic transition.

At pH 5.4, the retraction of ether spectra from 1092.48 cm $^{-1}$  was seen evidently, and the peak shifted by 36 cm $^{-1}$ . The vibration registered at 1056 cm $^{-1}$  corresponds to the C–C skeleton of the cyclohexane. The addition of acid catalyzes ether cleavage and activates  $S_N2$  reaction to form alkyl halide and alcohol [109]. Angular deformation vibration for C–Cl was observed at 719.91 cm $^{-1}$  and that for alcohol overlapped with the hydroxyl spectrum at 3375.94 cm $^{-1}$ , in the presence of nucleophile (water). The morphological changes over pH change produced evidence for aberrations in the NSV5 $_{SolC24}$  at pH 6.8, while at pH 5.4, the shell surface ruptured (Fig. 12), hence the burst in the DNP release profile.

The finding proposed that the NSV5 $_{\rm SolC24}$  developed being pH-sensitive, cannot bypass the skin barrier as intact niosomes. The acidic pH of the skin protonates the carbonyl oxygen of the S60 ester group and the ether oxygen of the SolC24 and ruptures the niosome to facilitate drug release at the skin surface. To overcome this critical bottleneck, the solid MNs can be effectively employed not only to bypass this pH barrier but also to the skin barrier owing to its mechanical strength.

#### 3.10. Ex-vivo permeation studies of niosomes through MN

The comparative *in vitro* porcine skin permeation profile of intact NSV5 $_{\rm SolC24}$  for passive (without MN) and active (MN assisted) methods are shown in Fig. 14. The possible mechanism of skin permeation of intact NSV5 $_{\rm SolC24}$  is illustrated in Fig. 15.

It is significant to note that the skin treated with NSV5<sub>SolC24</sub> by the passive method permeated 529.835  $\pm$  88.833 µg of DNP (24 h) in overall. Of this, 95.5% of the DNP was released as a free drug from NSV5<sub>SolC24</sub> (collected as filtrate), thus displaying the evident role of surfactant, S60, and CHOL as a permeation enhancer. Surfactants also have the potential to solubilize the stratum corneum lipid layer [110]. The molecular dispersion of the drug in S60 enhances the partition coefficient, and the lipophilicity thereby improves the permeability [111]. The CHOL is known to facilitate the fusion of the niosome in the lipid bilayer of stratum corneum, disruption of the niosome, and increase their deposition in the skin [112]. Outwardly, the interaction can occur either at the skin surface or in the deeper dermal layers. And, it depends on the elasticity and deformability of the niosome. The physicochemical characteristic-size, charge, elasticity is also known to have a profound effect in enhancing the drug permeation [113]. The synergetic effect between NSV5<sub>SolC24</sub> formulation and the skin composition is believed to be responsible for improved skin permeation.

In contrast, the skin passive treated with an equivalent amount of DNP suspended in PBS, permeated  $21.73\pm2.86~\mu g$  for 24 h, which confirms that the chemical composition of the NSV5\_{SolC24} dictates the permeation parameters. Currently, it is understood that dermal penetration of the nanoparticle is size-dependent. The nanoparticles of size <20 nm can infiltrate as intact; nanoparticles <45 nm can permeate via damaged skin, and larger nanoparticles are freighted via the skin appendage [114–116]. Hence, the possible permeation of intact NSV5\_{SolC24} of size 180.1  $\pm$  1.83 nm carrying a DNP cargo of 23.436  $\pm$  3.575  $\mu g$  by the passive method is due to the shunted appendage route via the hair follicle canal. The result is in agreement with the research reported by the Lademann group for transdermal delivery of fluorescent dye loaded particles of 320 nm via the follicular hair route [115].

Undoubtedly, the passive treatment of the skin with NSV5<sub>SolC24</sub> would enhance the systemic absorption of the DNP. However, the skin with stratum corneum (porcine ear skin:14–30  $\mu m$ ) is a formidable barrier for trafficking of intact NSV5<sub>SolC24</sub> beyond which systemic translocation can manifest itself under specific scenarios. For penetration of NSV5<sub>SolC24</sub> measuring 180.1  $\pm$  1.83 nm into the viable epidermis, it is imperative to disrupt the physical barrier. Hence, MNs of varying length was adopted to subjugate the resistance offered by upper strata. The amount of DNP permeated as intact NSV5<sub>SolC24</sub>, and other permeation parameters are presented in Table 4.

A significant increase in the permeation of intact NSV5<sub>SolC24</sub> was ascertained for MN assisted active drug permeation when compared with the passive method. The cumulative DNP permeated over 24 h increased by 2.21, 4.45, and 26.46-fold with MN600, MN777, and MN1200, respectively, when compared to the passive permeation. A similar trend was demonstrated for Kp, Js, and ER values (Table 4). The flux value was found to be in the order of MN1200 > MN777 > MN600 > Passive. Despite low needle density in MN1200, a 26-fold shoot in the flux was observed with MN 1200 over the passive treatment. The enhancement in the permeation parameters can be attributed to the length of the MNs and not the needle density. The MN1200 with a needle length of 1100  $\mu m$  and needle density of 43 in 1 cm<sup>2</sup> showed better permeation when compared with MN600 with 500 µm needle length and 187 needles in 1 cm<sup>2</sup> active area. From the results, it is evident that with the increase in the height of the MNs, the penetration depth also increased to form micro-conduits, which facilitated enhanced permeation of intact  $NSV5_{SolC24}$  across the skin. The result was also supported by the overlayed-HPLC chromatogram (Fig. 16) obtained for the filtrates from the receptor compartment after 2h of treatment.

HPLC analysis showed a sharp peak for the free drug from passive treated  $NSV5_{SolC24}$  at a retention time of 6.8min. However, MN-assisted filtrates showed no signs of free DNP in the filtrate (Fig. 16), which validated the fact that MNs can be effectively used in the translocating the intact  $NSV5_{SolC24}$ . Besides, the stability, the charge (-32.7 mV), and

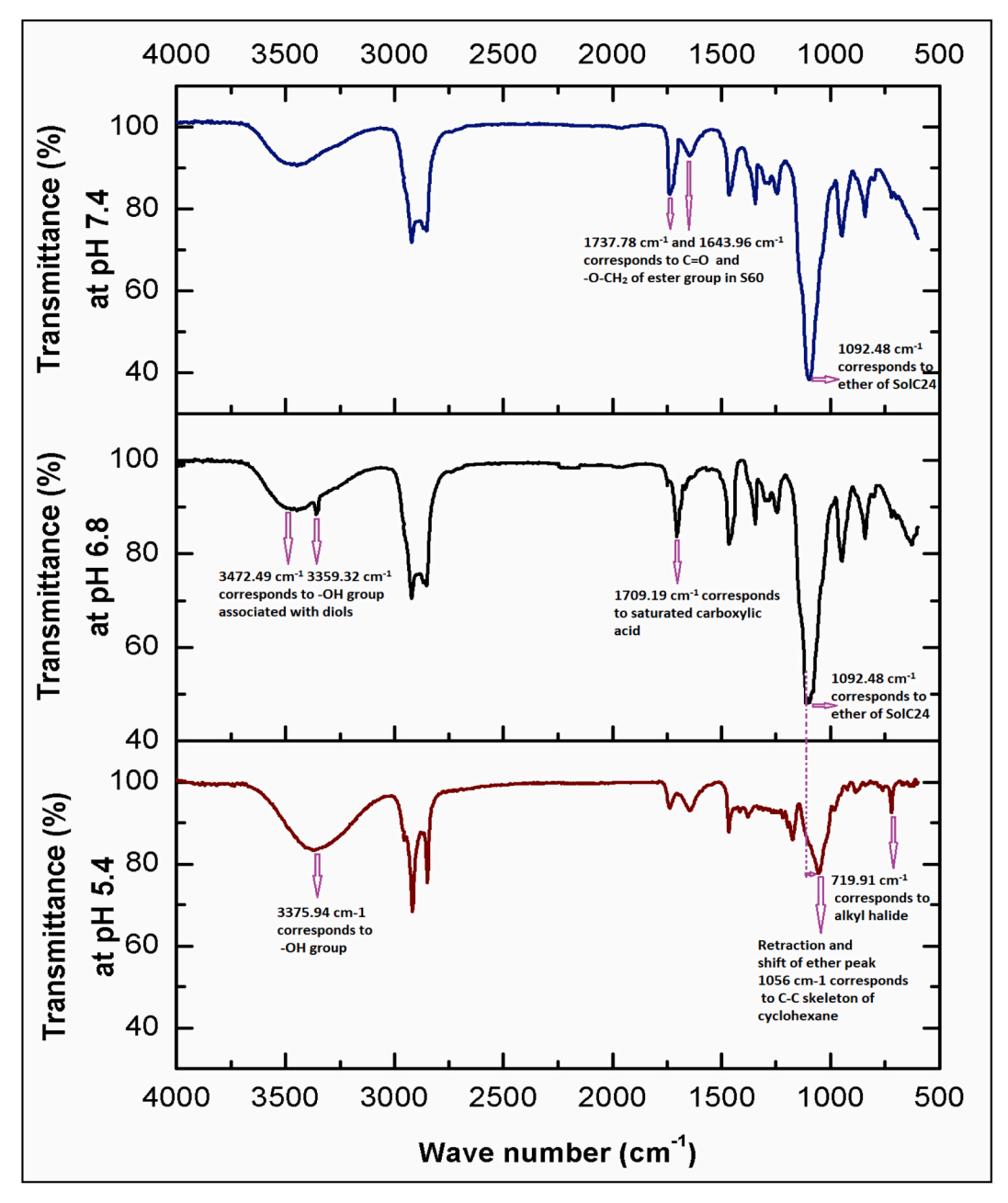


Fig. 13. Comparative FTIR spectra of lyophilized NSV5<sub>SolC24</sub> at different physiological pH.

the size (180.1 nm) of NSV5 $_{SolC24}$  favored MN assisted transdermal delivery beyond stratum cornea. The observation suggested that the pH-sensitive NSV5 $_{SolC24}$  can be effectively used to deliver the DNP across the skin barrier and efficiently translocate intact pH-sensitive NSV5 $_{SolC24}$  when assisted with MNs, thus promoting the release of DNP when countered by the acidic microenvironment.

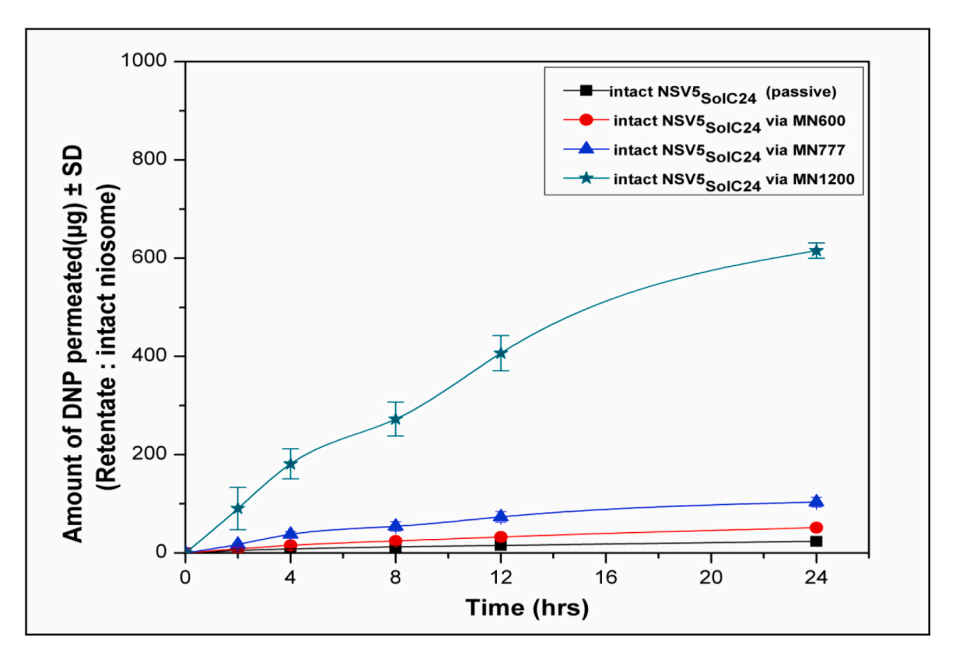
An improved retention of such intact niosome in the brain blood capillaries joined with an adsorption to the capillary wall, both concurring would enhance the drug transport across the endothelial cell layer by increasing the concentration gradient [117]. A possible surfactant effect could be also considered, characterized by a solubilization of the endothelial cell membrane lipids, leading to membrane fluidization and increased drug permeation through the BBB [117]. A further possibility could be the endocytosis of intact niosome by the endothelial cells, followed by the delivery of the drug within these cells and then delivery to the brain [118]. All of these mechanisms also could operate in combination. Hence, MN-assisted transdermal administration of DNP

niosomes can be a practical approach for delivering drugs to the brain by crossing BBB, and thus can be used in the treatment of brain-related disorders.

In the frame of reference to the DNP content in the treated skin, analogy for the translocation intact  $NSV5_{SolC24}$  within/across the skin could not to established as there was no means to isolate the intact  $NSV5_{SolC24}$  from the free DNP. However, a significantly higher amount of DNP was found to be deposited in the skin treated with the MNs at the end of 24 h and is a testimony to potential DNP skin deposition.

#### 4. Conclusions

The study demonstrated the interdependence of process and formulation variables on the physicochemical properties of the niosome. The *in vitro* release studies, FTIR studies, and the morphological conformation of NSV5 $_{\rm SolC24}$  constituted evidence that the optimized formulation is pH-sensitive. The prolonged circulation of niosomes in



 $\textbf{Fig. 14.} \ \ \text{Comparative DNP permeation profile of intact NSV5}_{SolC24} \ \ \text{for passive and MN-assisted active methods}.$ 

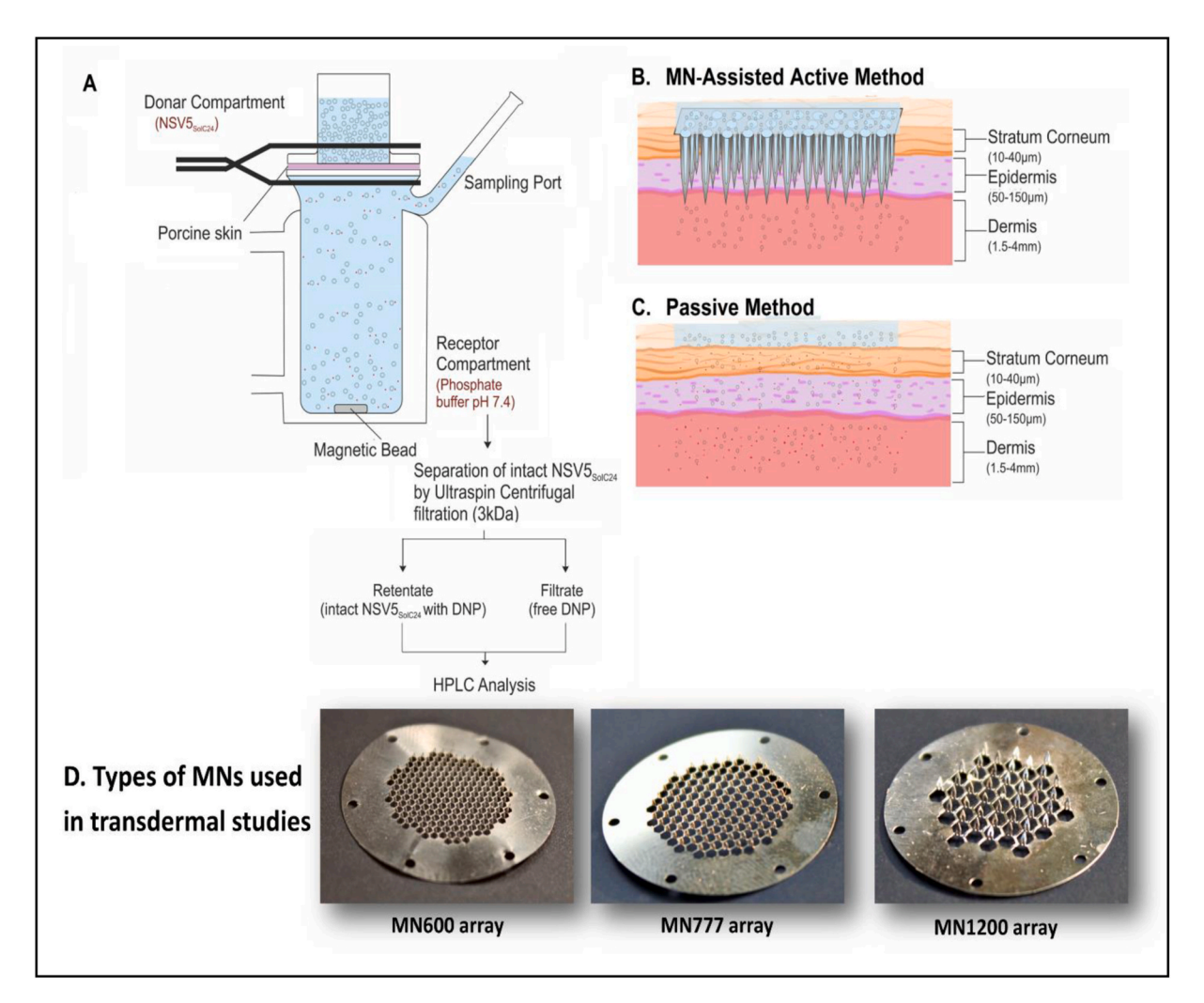


Fig. 15. Schematic representation for (A) in vitro porcine skin permeation studies using Franz Diffusion Cell. (B) the mechanism involved in the MN-assisted active method. (C) the mechanism involved in the passive method. (D) MNs used for the transdermal studies.

Table 4 Permeation parameters for intact NSV5  $_{SolC24}$  in the retentate  $^{a}$  in 24 h.

Skin treated with	Cumulative DNP permeated	Flux, $J_s$ ( $\mu g/cm^2/h$ )	Permeability coefficient, $K_p x 10^{-5} (cm/h)$	ER	DNP in porcine skin (μg) <sup>b</sup>
Passive					_
NSV5 <sub>SolC24</sub>	$23.43 \pm 3.57$	$0.391\pm0.08$	$24.40 \pm 5.96$	1	$792.09 \pm 19.31$
Active					
$MN600 + NSV5_{SolC24}$	$51.31 \pm 4.43$	$0.855\pm0.10$	$54.29 \pm 8.29$	$2.21\pm0.21$	$2531.05 \pm 184.47$
$MN777 + NSV5_{SolC24}$	$103.42 \pm 9.87$	$1.723\pm0.23$	$113.26 \pm 19.4$	$4.45\pm0.36$	$1467.59 \pm 156.53$
$MN1200 + NSV5_{SolC24}$	$608.19\pm15.6$	$10.136\pm1.54$	$995.15 \pm 98.78$	$26.46\pm4.7$	$2390.41 \pm 173.34$

MN Specifications: MN600-500 μm and 187needle/cm², MN777-700 μm and 121needle/cm² and MN1200- 1100 μm and 43needle/cm².

 $<sup>^{\</sup>rm b}$  Skin area = 2.5 sq cm.

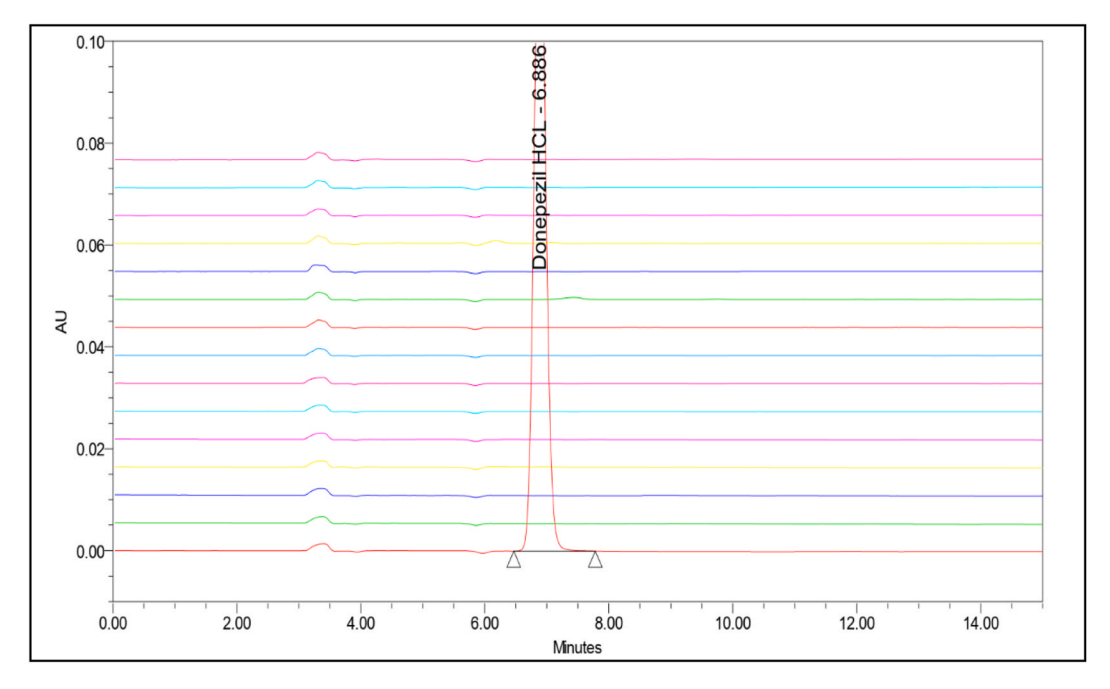


Fig. 16. Overlayed-HPLC chromatogram for the free drug in the filtrate (receptor compartment after 2 h of treatment) for passive against MN assisted delivery.

the blood helps in distributing the drug to the brain wherein the rapid release of the DNP is expected. MNs fostered improvement in transdermal permeation of intact  $\rm NSV5_{SolC24}$  across porcine ear skin, irrespective of MN length. It may be inferred that it is feasible to deliver the intact  $\rm NSV5_{SolC24}$  using MNs across the skin by a rather painless and noninvasive method, thereby improving patient compliance. These positive results also suggest that the proposed MN-assisted DNP niosome delivery method could be successfully used to deliver niosomes to the brain through systemic circulation and can be used as an alternative to current therapy. Further preclinical and clinical studies are to be carried out to prove the  $in\ vivo\ efficacy$ .

## CRediT authorship contribution statement

Archana S. Nayak: Project administration, Conceptualization, Writing - original draft, Visualization. Srivani Chodisetti: Data curation. Shivaprasad Gadag: Data curation. Usha Yogendra Nayak: Writing - review & editing, Supervision, Project administration. Srinikethan Govindan: Project administration, Conceptualization, Data curation, Supervision, Project administration. Keyur Raval: Supervision, Project administration, Formal analysis.

## Declaration of competing interest

The authors declare that they have no known competing financial interests or personal relationships that could have appeared to influence the work reported in this paper.

## Acknowledgments

The authors are thankful to National Institute of Technology Karnataka, India for providing financial support. We are grateful to cryo FEG- SEM Lab, IIT Bombay, for their technical assistance. We extend our gratitude to STIC, CUSAT, Cochin University, for providing the HR-TEM imaging facility. We would like to acknowledge the Dept. of Pharmaceutics, MAHE, Manipal, for providing consistent support to carry out this work.

## Appendix A. Supplementary data

Supplementary data to this article can be found online at https://doi.org/10.1016/j.jddst.2020.101945.

#### References

- J.T. Coyle, D.L. Price, M.R. DeLong, Alzheimer's disease: a disorder of cortical cholinergic innervation, Science 80 (219) (1983) 1184–1190, https://doi.org/ 10.1126/science.6338589.
- [2] M.B. Colovic, D.Z. Krstic, T.D. Lazarevic-Pasti, A.M. Bondzic, V.M. Vasic, Acetylcholinesterase inhibitors: pharmacology and toxicology, Curr. Neuropharmacol. 11 (2013) 315–335, https://doi.org/10.2174/ 1570159X11311030006.
- [3] C. Christodoulou, P. Melville, W.F. Scherl, W.S. MacAllister, L.E. Elkins, L. B. Krupp, Effects of donepezil on memory and cognition in multiple sclerosis, J. Neurol. Sci. 245 (2006) 127–136, https://doi.org/10.1016/j.jns.2005.08.021.

<sup>&</sup>lt;sup>a</sup> after centrifugal filtration (3 kDa MWCO), retentate with intact NSV5<sub>SolC24</sub> was considered.

- [4] D.G. Wilkinson, The pharmacology of donepezil: a new treatment for Alzheimer's disease, Expet Opin. Pharmacother. 1 (1999) 121–135.
- [5] R.S. Muramatsu, M.H.J. Litzinger, J. Takeshita Ed Fisher, Alternative formulations, delivery methods, and administration options for psychotropic medications in elderly patients with behavioral and psychological symptoms of dementia, Am. J. Geriatr. Pharmacother. (2010) 98–114, https://doi.org/ 10.1016/j.amjopharm.2010.03.003.
- [6] M. Mehta, A. Adem, M. Sabbagh, M. M, A. A, New acetylcholinesterase inhibitors for Alzheimer's disease, Int. J. Alzheimer's Dis. 2012 (2012) 728983, https://doi. org/10.1155/2012/728983.
- [7] S. Md, M. Ali, R. Ali, A. Bhatnagar, S. Baboota, J. Ali, Donepezil nanosuspension intended for nose to brain targeting: in vitro and in vivo safety evaluation, Int. J. Biol. Macromol. 67 (2014) 418–425, https://doi.org/10.1016/j. ijbiomac.2014.03.022.
- [8] A.K. Al Asmari, Z. Ullah, M. Tariq, A. Fatani, Preparation, characterization, and in vivo evaluation of intranasally administered liposomal formulation of donepezil, Drug Des. Dev. Ther. 10 (2016) 205, https://doi.org/10.2147/DDDT.S93937.
- [9] S. Al Harthi, S.E. Alavi, M.A. Radwan, M.M. El Khatib, I.A. AlSarra, Nasal delivery of donepezil HCl-loaded hydrogels for the treatment of Alzheimer's disease, Sci. Rep. 9 (2019) 1–20, https://doi.org/10.1038/s41598-019-46032-y.
- [10] M. Yasir, U.V.S. Sara, I. Chauhan, P.K. Gaur, A.P. Singh, D. Puri, A. Ameeduzzafar, Solid lipid nanoparticles for nose to brain delivery of donepezil: formulation, optimization by Box–Behnken design, in vitro and in vivo evaluation, Artif. Cells, Nanomedicine Biotechnol 46 (2018) 1838–1851, https:// doi.org/10.1080/21691401.2017.1394872.
- [11] L. Illum, Is nose-to-brain transport of drugs in man a reality? J. Pharm. Pharmacol. 56 (2004) 3–17, https://doi.org/10.1211/0022357022539.
- [12] B. Bhavna, M. Shadab, M. Ali, S. Baboota, J.K. Sahni, A. Bhatnagar, J. Ali, Preparation, characterization, in vivo biodistribution and pharmacokinetic studies of donepezil-loaded PLGA nanoparticles for brain targeting, Drug Dev. Ind. Pharm. 40 (2014) 278–287, https://doi.org/10.3109/ 03639045.2012.758130.
- [13] Y.H. Kim, H.Y. Choi, H.S. Lim, S.H. Lee, H.S. Jeon, D. Hong, S.S. Kim, Y.K. Choi, K.S. Bae, Single dose pharmacokinetics of the novel transdermal donepezil patch in healthy volunteers, Drug Des. Dev. Ther. 9 (2015) 1419–1426, https://doi.org/ 10.2147/DDDT.S78555.
- [14] R.K. Subedi, J.P. Ryoo, C. Moon, M.K. Chun, H.K. Choi, Formulation and in vitro evaluation of transdermal drug delivery system for donepezil, J. Pharm. Investig. 42 (2012) 1–7, https://doi.org/10.1007/s40005-012-0002-y.
- [15] B. Nalluri, S.V. Anusha, S. Bramhini, J. Amulya, A. Sultana, C. Teja, D. Das, In vitro skin permeation enhancement of sumatriptan by microneedle application, Curr. Drug Deliv. 12 (2015) 761–769, https://doi.org/10.2174/1567201812666150304123150.
- [16] R. Kumar, A. Philip, Modified transdermal technologies: breaking the barriers of drug permeation via the skin, Trop. J. Pharmaceut. Res. 6 (2007) 633–644, https://doi.org/10.4314/tipr.v6i1.14641.
- [17] J.W. Lee, M.R. Han, J.H. Park, Polymer microneedles for transdermal drug delivery, J. Drug Target. 21 (2013) 211–223, https://doi.org/10.3109/ 1061186X 2012 741136
- [18] C.P. Zhou, Y.L. Liu, H.L. Wang, P.X. Zhang, J.L. Zhang, Transdermal delivery of insulin using microneedle rollers in vivo, Int. J. Pharm. 392 (2010) 127–133, https://doi.org/10.1016/j.ijpharm.2010.03.041.
- [19] M.C. Kearney, E. Caffarel-Salvador, S.J. Fallows, H.O. McCarthy, R.F. Donnelly, Microneedle-mediated delivery of donepezil: potential for improved treatment options in Alzheimer's disease, Eur. J. Pharm. Biopharm. 103 (2016) 43–50, https://doi.org/10.1016/j.ejpb.2016.03.026.
- [20] J.Y. Kim, M.R. Han, Y.H. Kim, S.W. Shin, S.Y. Nam, J.H. Park, Tip-loaded dissolving microneedles for transdermal delivery of donepezil hydrochloride for treatment of Alzheimer's disease, Eur. J. Pharm. Biopharm. 105 (2016) 148–155, https://doi.org/10.1016/j.ejpb.2016.06.006.
- [21] N. Bertrand, J. Wu, X. Xu, N. Kamaly, O.C. Farokhzad, Cancer nanotechnology: the impact of passive and active targeting in the era of modern cancer biology, Adv. Drug Deliv. Rev. 66 (2014) 2–25, https://doi.org/10.1016/j. addr 2013 11 009
- [22] D. Prema, J. Prakash, S. Vignesh, P. Veluchamy, C. Ramachandran, D.B. Samal, D. H. Oh, S. Sahabudeen, G.D. Venkatasubbu, Mechanism of inhibition of graphene oxide/zinc oxide nanocomposite against wound infection causing pathogens, Appl. Nanosci. 10 (2020) 827–849, https://doi.org/10.1007/s13204-019-01152-0
- [23] J.Y. Fang, S.Y. Yu, P.C. Wu, Y. Bin Huang, Y.H. Tsai, In vitro skin permeation of estradiol from various proniosome formulations, Int. J. Pharm. 215 (2001) 91–99, https://doi.org/10.1016/S0378-5173(00)00669-4.
- [24] H.M. El-Laithy, O. Shoukry, L.G. Mahran, Novel sugar esters proniosomes for transdermal delivery of vinpocetine: preclinical and clinical studies, Eur. J. Pharm. Biopharm. 77 (2011) 43–55, https://doi.org/10.1016/j. eipb.2010.10.011.
- [25] S. Ghanbarzadeh, A. Khorrami, S. Arami, Nonionic surfactant-based vesicular system for transdermal drug delivery, Drug Deliv. 22 (2015) 1071–1077, https:// doi.org/10.3109/10717544.2013.873837.
- [26] J. Prakash, M. Venkatesan, G. Bharath, S. Anwer, P. Veluswamy, D. Prema, K. S. Venkataprasanna, G.D. Venkatasubbu, Investigations on the in vivo toxicity analysis of reduced graphene oxide/TiO2 nanocomposite in zebrafish embryo and larvae (Danio rerio), Appl. Surf. Sci. 481 (2019) 1360–1369, https://doi.org/10.1016/j.apsusc.2019.03.287.

- [27] P.E. Fraser, J.T. Nguyen, W.K. Surewicz, D.A. Kirschner, pH-dependent structural transitions of Alzheimer amyloid peptides, Biophys. J. 60 (1991) 1190–1201, https://doi.org/10.1016/S0006-3495(91)82154-3.
- [28] C.S. Atwood, R.D. Moir, X. Huang, R.C. Scarpa, N.M.E. Bacarra, D.M. Romano, M. A. Hartshorn, R.E. Tanzi, A.I. Bush, Dramatic aggregation of alzheimer by Cu(II) is induced by conditions representing physiological acidosis, J. Biol. Chem. 273 (1998) 12817–12826, https://doi.org/10.1074/jbc.273.21.12817.
- [29] P. Arunothayanun, M.S. Bernard, D.Q.M. Craig, I.F. Uchegbu, A.T. Florence, The effect of processing variables on the physical characteristics of non-ionic surfactant vesicles (niosomes) formed from a hexadecyl diglycerol ether, Int. J. Pharm. 201 (2000) 7–14, https://doi.org/10.1016/S0378-5173(00)00362-8.
- [30] M. Bragagni, N. Mennini, C. Ghelardini, P. Mura, Development and characterization of niosomal formulations of doxorubicin aimed at brain targeting, J. Pharm. Pharmaceut. Sci. 15 (2012) 184–196, https://doi.org/ 10.18433/12330M
- [31] I.A. Darwish, I.F. Uchegbu, The evaluation of crown ether based niosomes as cation containing and cation sensitive drug delivery systems, Int. J. Pharm. 159 (1997) 207–213, https://doi.org/10.1016/S0378-5173(97)00289-5.
- [32] I.F. Uchegbu, A.T. Florence, Non-ionic surfactant vesicles (niosomes): physical and pharmaceutical chemistry, Adv. Colloid Interface Sci. 58 (1995) 1–55, https://doi.org/10.1016/0001-8686(95)00242-I.
- [33] T.-L. Ho, G.A. Olah, Cleavage of esters and ethers with iodotrimethylsilane, Angew Chem. Int. Ed. Engl. 15 (1976) 774–775, https://doi.org/10.1002/ anie.197607741.
- [34] R.W. Jackson, A mild and selective method for the cleavage of tert-butyl esters, Tetrahedron Lett. 42 (2001) 5163–5165, https://doi.org/10.1016/S0040-4039 (01)00980-7
- [35] T. Kokubo, H. Takadama, How useful is SBF in predicting in vivo bone bioactivity? Biomaterials 27 (2006) 2907–2915.
- [36] K. Ruckmani, V. Sankar, Formulation and optimization of zidovudine niosomes, AAPS PharmSciTech 11 (2010) 1119–1127, https://doi.org/10.1208/s12249-010-9480-2.
- [37] I.F. Uchegbu, J.A. Turton, J.A. Double, A.T. Florence, Drug distribution and a pulmonary adverse effect of intraperitoneally administered doxorubicin niosomes in the mouse, Biopharm Drug Dispos. 15 (1994) 691–707, https://doi.org/ 10.1002/bdd.2510150807.
- [38] P.S. Jadon, V. Gajbhiye, R.S. Jadon, K.R. Gajbhiye, N. Ganesh, Enhanced oral bioavailability of griseofulvin via niosomes, AAPS PharmSciTech 10 (2009) 1186–1192, https://doi.org/10.1208/s12249-009-9325-z.
- [39] S. Jain, B.H. Chaudhari, N.K. Swarnakar, Preparation and characterization of niosomal gel for iontophoresis mediated transdermal delivery of isosorbide dinitrate, Drug Deliv. Transl. Res. 1 (2011) 309–321, https://doi.org/10.1007/ s13346-011-0035-1.
- [40] T. Senthil Kumar, P. Solairaj, A. Thangathirupathi, Analytical method development and validation of donepezil hydrochloride tablets by RP-HPLC, Int. J. Pharm. Pharmaceut. Sci. 3 (2011) 62–65.
- [41] M.Y. Levy, S. Benita, Drug release from submicronized o/w emulsion: a new in vitro kinetic evaluation model, Int. J. Pharm. 66 (1990) 29–37, https://doi.org/ 10.1016/0378-5173(90)90381-D.
- [42] C. Washington, Drug release from microdisperse systems: a critical review, Int. J. Pharm. 58 (1990) 1–12, https://doi.org/10.1016/0378-5173(90)90280-H.
- [43] U. Jacobi, M. Kaiser, R. Toll, S. Mangelsdorf, H. Audring, N. Otberg, W. Sterry, J. Lademann, Porcine ear skin: an in vitro model for human skin, Skin Res. Technol. 13 (2007) 19–24, https://doi.org/10.1111/j.1600-0846.2006.00179.x.
- [44] G.A. Simon, H.I. Maibach, The pig as an experimental animal model of percutaneous permeation in man: qualitative and quantitative observations - an overview, Skin Pharmacol. Appl. Skin Physiol. 13 (2000) 229–234, https://doi. org/10.1159/000029928
- [45] V. Leeladurga, U.C. Teja, S.K.A. Sultana, K. Sudeep, V.S.S. Anusha, T. Han, B. N. Nalluri, D.B. Das, Application of microneedle arrays for enhancement of transdermal permeation of insulin: in vitro experiments, scaling analyses and numerical simulations, AAPS PharmSciTech 17 (2016) 915–922, https://doi.org/10.1208/s12249-015-0416-8.
- [46] Guideline, ICH Harmonised Tripartite, Stability testing of new drug substances and products, Q1A (R2), current step 4 (2003) 1–24, https://doi.org/10.1136/ bmi.333.7574.873-a.
- [47] B. Mukherjee, B. Patra, B. Layek, A. Mukherjee, Sustained release of acyclovir from nano-liposomes and nano-niosomes: an in vitro study, Int. J. Nanomed. 2 (2007) 213.
- [48] G.S. Asthana, P.K. Sharma, A. Asthana, In vitro and in vivo evaluation of niosomal formulation for controlled delivery of clarithromycin, Sci. Tech. Rep. (2016) 2016, https://doi.org/10.1155/2016/6492953.
- [49] D. Akhilesh, K. Bini, J. Kamath, Review on span-60 based non-ionic surfactant vesicles (niosomes) as novel drug delivery, Int. J. Res. Pharm. Biomed. Sci. 3 (2012) 6–12.
- [50] C.A. Hunter, T.F. Dolan, G.H. Coombs, A.J. Baillie, Vesicular systems (niosomes and liposomes) for delivery of sodium stibogluconate in experimental murine visceral leishmaniasis, J. Pharm. Pharmacol. 40 (1988) 161–165, https://doi.org/ 10.1111/j.2042-7158.1988.tb05210.x.
- [51] E. Essa, Effect of formulation and processing variables on the particle size of sorbitan monopalmitate niosomes, Asian J. Pharm. 4 (2010) 227, https://doi.org/ 10.4103/0973-8398.76752.
- [52] T. Helgason, T.S. Awad, K. Kristbergsson, D.J. McClements, J. Weiss, Effect of surfactant surface coverage on formation of solid lipid nanoparticles (SLN), J. Colloid Interface Sci. 334 (2009) 75–81, https://doi.org/10.1016/j. jcis.2009.03.012.

- [53] J.N. Israelachvili, S. Marcelja, R.G. Horn, J.N. Israelachvili, Physical principles of membrane organization, Q. Rev. Biophys. 13 (1980) 121–200, https://doi.org/ 10.1017/S0033583500001645.
- [54] J.N. Israelachvili, D.J. Mitchell, B.W. Ninham, Theory of self-assembly of hydrocarbon amphiphiles into micelles and bilayers, J. Chem. Soc. Faraday Trans. 2 Mol. Chem. Phys. 72 (1976) 1525–1568, https://doi.org/10.1039/ F29767201525.
- [55] D. Jurašin, M. Vinceković, A. Pustak, I. Šmit, M. Bujan, N. Filipović-Vinceković, Lamellar to hexagonal columnar liquid crystalline phase transition in a catanionic surfactant mixture: dodecylammonium chloride-sodium bis(2-ethylhexyl) sulfosuccinate, Soft Matter 9 (2013) 3349–3360, https://doi.org/10.1039/ c3sm27665a.
- [56] T. Yoshioka, B. Sternberg, A.T. Florence, Preparation and properties of vesicles (niosomes) of sorbitan monoesters (Span 20, 40, 60 and 80) and a sorbitan triester (Span 85), Int. J. Pharm. 105 (1994) 1–6, https://doi.org/10.1016/0378-5173(94)90228-3.
- [57] D.J. Mitchell, B.W. Ninham, Micelles, vesicles and microemulsions, J. Chem. Soc. Faraday Trans. 2 Mol. Chem. Phys. 77 (1981) 601–629, https://doi.org/10.1039/ F29817700601.
- [58] I.F. Uchegbu, S.P. Vyas, Non-ionic surfactant based vesicles (niosomes) in drug delivery, Int. J. Pharm. 172 (1998) 33–70, https://doi.org/10.1016/S0378-5173 (98)00169-0.
- [59] S. Khoee, M. Yaghoobian, An investigation into the role of surfactants in controlling particle size of polymeric nanocapsules containing penicillin-G in double emulsion, Eur. J. Med. Chem. 44 (2009) 2392–2399, https://doi.org/ 10.1016/j.ejmech.2008.09.045.
- [60] M.I. Khan, A. Madni, S. Ahmad, M.A. Mahmood, M. Rehman, M. Ashfaq, Formulation design and characterization of a non-ionic surfactant based vesicular system for the sustained delivery of a new chondroprotective agent, Brazilian J. Pharm. Sci. 51 (2015) 607–616, https://doi.org/10.1590/S1984-2250201500020012
- [61] A.S. Guinedi, N.D. Mortada, S. Mansour, R.M. Hathout, Preparation and evaluation of reverse-phase evaporation and multilamellar niosomes as ophthalmic carriers of acetazolamide, Int. J. Pharm. 306 (2005) 71–82, https:// doi.org/10.1016/j.ijpharm.2005.09.023.
- [62] K.M. Kazi, A.S. Mandal, N. Biswas, A. Guha, S. Chatterjee, M. Behera, K. Kuotsu, Niosome: a future of targeted drug delivery systems, "J. Adv. Pharm. Technol. Research" (JAPTR)" 1 (2010) 374–380.
- [63] J.W. Cooper, C. Gunn, Cooper and gunn's dispensing for pharmaceutical students, Med. J. Aust. (1966), https://doi.org/10.5694/j.1326-5377.1966.tb72707.x.
- [64] K.V.R. Reddy, K. Sravani, S.T.P. Vaishnavi, U. Srilatha, R. Srilatha, M. Poornima, V.B. Reddy, K. Navaneetha, Factors affecting in formation of niosomes, Indo Am. J. Pharm. Res. 4 (2014) 2087–2091.
- [65] D. Needham, R.S. Nunn, Elastic deformation and failure of lipid bilayer membranes containing cholesterol, Biophys. J. 58 (1990) 997–1009, https://doi. org/10.1016/S0006-3495(90)82444-9.
- [66] S.C. Lee, K.E. Lee, J.J. Kim, S.H. Lim, The effect of cholesterol in the liposome bilayer on the stabilization of incorporated retinol, J. Liposome Res. 15 (2005) 157–166, https://doi.org/10.1080/08982100500364131.
- [67] S. Raffy, J. Teissié, Control of lipid membrane stability by cholesterol content, Biophys. J. 76 (1999) 2072–2080, https://doi.org/10.1016/S0006-3495(99)
- [68] M.R. Vist, J.H. Davis, Phase equilibria of cholesterol/ dipalmitoylphosphatidylcholine mixtures: 2H nuclear magnetic resonance and differential scanning calorimetry, Biochemistry 29 (1990) 451–464, https://doi. org/10.1021/bi00454a021
- [69] L. Redondo-Morata, M.I. Giannotti, F. Sanz, Influence of cholesterol on the phase transition of lipid bilayers: a temperature-controlled force spectroscopy study, Langmuir 28 (2012) 12851–12860, https://doi.org/10.1021/la302620t.
- [70] C. Bernsdorff, A. Wolf, R. Winter, E. Gratton, Effect of hydrostatic pressure on water penetration and rotational dynamics in phospholipid-cholesterol bilayers, Biophys. J. 73 (1997) 1264, https://doi.org/10.1016/S0006-3495(97)78773-3.
- [71] C. Kirby, J. Clarke, G. Gregoriadis, Effect of the cholesterol content of small unilamellar liposomes on their stability in vivo and in vitro, Biochem. J. 186 (1980) 591–598, https://doi.org/10.1042/bj1860591.
- [72] P. Balakrishnan, S. Shanmugam, W.S. Lee, W.M. Lee, J.O. Kim, D.H. Oh, D. D. Kim, J.S. Kim, B.K. Yoo, H.G. Choi, J.S. Woo, C.S. Yong, Formulation and in vitro assessment of minoxidil niosomes for enhanced skin delivery, Int. J. Pharm. 377 (2009) 1–8, https://doi.org/10.1016/j.ijpharm.2009.04.020.
- [73] M.S. El-Samaligy, N.N. Afifi, E.A. Mahmoud, Evaluation of hybrid liposomesencapsulated silymarin regarding physical stability and in vivo performance, Int. J. Pharm. 319 (2006) 121–129, https://doi.org/10.1016/j.ijpharm.2006.04.023.
- [74] Y. Hao, F. Zhao, N. Li, Y. Yang, K. Li, Studies on a High Encapsulation of Colchicine by a Niosome System, vol. 244, 2002, pp. 73–80.
- [75] E.S. Richardson, W.G. Pitt, D.J. Woodbury, The role of cavitation in liposome formation, Biophys. J. 93 (2007) 4100–4107, https://doi.org/10.1529/ biophysi.107.104042.
- [76] D.D. Lasic, Mechanisms of liposome formation, J. Liposome Res. 5 (1995) 431–441, https://doi.org/10.3109/08982109509010233.
- [77] C.E. Brennen, Cavitation and Bubble Dynamics, Cambridge University Press, 2014, https://doi.org/10.1017/CBO9781107338760.
- [78] V.A. Hackley, M.R. Wiesner, Protocol for preparation of nanoparticle dispersions from powdered material using ultrasonic disruption, CEINT, Natl. Inst. Standars Technol. (2010), https://doi.org/10.6028/NIST.SP.1200-2.

- [79] J.S. Taurozzi, V.A. Hackley, M.R. Wiesner, Preparation of nanoparticle dispersions from powdered material using ultrasonic disruption, NIST - Spec. Publ. 1200 (2012) 1200–1202.
- [80] D.D. Lasic, Liposomes: from Physics to Applications, Elsevier Sci. Publ. B. V., 1993
- [81] G.V. Betageri, D.L. Parsons, Drug encapsulation and release from multilamellar and unilamellar liposomes, Int. J. Pharm. 81 (1992) 235–241, https://doi.org/ 10.1016/0378-5173(92)90015-T.
- [82] M. Winterhalter, D.D. Lasic, Liposome stability and formation: experimental parameters and theories on the size distribution, Chem. Phys. Lipids 64 (1993) 35–43, https://doi.org/10.1016/0009-3084(93)90056-9.
- [83] W. Helfrich, The size of bilayer vesicles generated by sonication, Phys. Lett. 50 (1974) 115–116, https://doi.org/10.1016/0375-9601(74)90899-8.
- [84] I. León, R. Montero, A. Longarte, J.A. Fernández, Influence of dispersive forces on the final shape of a reverse micelle, Phys. Chem. Chem. Phys. 17 (2015) 2241–2245, https://doi.org/10.1039/c4cp03667k.
- [85] E.M. Oriyama, T.S. Aito, Y.T. Okuoka, Evaluation of the hardness of lipid bilayer membranes of liposomes by the ultrasound attenuation method, Society 52 (2003) 433–437, https://doi.org/10.5650/jos.52.433.
- [86] C.P. Jain, S.P. Vyas, Preparation and characterization of niosomes containing rifampicin for lung targeting, J. Microencapsul. 12 (1995) 401–407, https://doi. org/10.3109/02652049509087252.
- [87] M.M.A.E. Claessens, B.F. Van Oort, F.A.M. Leermakers, F.A. Hoekstra, M.A. C. Stuart, Charged lipid vesicles: effects of salts on bending rigidity, stability, and size, Biophys. J. 87 (2004) 3882–3893, https://doi.org/10.1529/ biophys.103.036772
- [88] M.M. Mehanna, N.A. El-Kader, M.W. Samaha, Liposomes as potential carriers for ketorolac ophthalmic delivery: formulation and stability issues, Brazilian J. Pharm. Sci. 53 (2017), https://doi.org/10.1590/s2175-97902017000216127.
- [89] V.B. Junyaprasert, V. Teeranachaideekul, T. Supaperm, Effect of charged and non-ionic membrane additives on physicochemical properties and stability of niosomes, AAPS PharmSciTech 9 (2008) 851–859, https://doi.org/10.1208/ s12249-008-9121-1.
- [90] G. Abdelbary, N. El-Gendy, Niosome-Encapsulated gentamicin for ophthalmic controlled delivery, AAPS PharmSciTech 9 (2008) 740–747, https://doi.org/ 10.1208/s12249-008-9105-1
- [91] M. Bragagni, N. Mennini, S. Furlanetto, S. Orlandini, C. Ghelardini, P. Mura, Development and characterization of functionalized niosomes for brain targeting of dynorphin-B, Eur. J. Pharm. Biopharm. 87 (2014) 73–79, https://doi.org/ 10.1016/j.ejpb.2014.01.006.
- [92] I.F. Uchegbu, J.A. Double, J.A. Turton, A.T. Florence, Distribution, metabolism and tumoricidal activity of doxorubicin administered in sorbitan monostearate (span 60) niosomes in the mouse, Pharm. Res. An Off. J. Am. Assoc. Pharm. Sci. 12 (1995) 1019–1024, https://doi.org/10.1023/A:1016210515134.
- [93] C. Dufes, J.C. Olivier, F. Gaillard, A. Gaillard, W. Couet, J.M. Muller, Brain delivery of vasoactive intestinal peptide (VIP) following nasal administration to rats, Int. J. Pharm. 255 (2003) 87–97.
- [94] C. Dufes, F. Gaillard, I.F. Uchegbu, A.G. Schätzlein, J.C. Olivier, J.M. Muller, Glucose-targeted niosomes deliver vasoactive intestinal peptide (VIP) to the brain, Int. J. Pharm. 285 (2004) 77–85, https://doi.org/10.1016/j. iipharm.2004.07.020.
- [95] M. Carafa, E. Santucci, G. Lucania, Lidocaine-loaded non-ionic surfactant vesicles: characterization and in vitro permeation studies, Int. J. Pharm. 231 (2002) 21–32. https://doi.org/10.1016/S0378-5173(01)00828-6.
- [96] J.Y. Fang, C.T. Hong, W.T. Chiu, Y.Y. Wang, Effect of liposomes and niosomes on skin permeation of enoxacin, Int. J. Pharm. 219 (2001) 61–72, https://doi.org/ 10.1016/S0378-5173(01)00627-5.
- [97] C.S. Chaw, K.Y.A. Kim, Effect of formulation compositions on niosomal preparations, Pharmaceut. Dev. Technol. 18 (2013) 667–672, https://doi.org/ 10.3109/10837450.2012.672988.
- [98] M. Carafa, E. Santucci, F. Alhaique, T. Coviello, E. Murtas, F.M. Riccieri, G. Lucania, M.R. Torrisi, Preparation and properties of new unilamellar nonionic/ionic surfactant vesicles, Int. J. Pharm. 160 (1998) 51–59, https://doi.org/ 10.1016/S0378-5173(97)00294-9.
- [99] H. Abdelkader, A.W.G. Alani, R.G. Alany, Recent advances in non-ionic surfactant vesicles (niosomes): self-assembly, fabrication, characterization, drug delivery applications and limitations, Drug Deliv. 21 (2014) 87–100, https://doi.org/ 10.3109/10717544.2013.838077.
- [100] H. Abdelkader, S. Ismail, A. Kamal, R.G. Alany, Design and evaluation of controlled-release niosomes and discomes for naltrexone hydrochloride ocular delivery, J. Pharmacol. Sci. 100 (2011) 1833–1846, https://doi.org/10.1002/ jps.22422.
- [101] A.Y. Waddad, S. Abbad, F. Yu, W.L.L. Munyendo, J. Wang, H. Lv, J. Zhou, Formulation, characterization and pharmacokinetics of Morin hydrate niosomes prepared from various non-ionic surfactants, Int. J. Pharm. 456 (2013) 446–458, https://doi.org/10.1016/j.ijpharm.2013.08.040.
- [102] C. Dufes, a G. Schätzlein, L. Tetley, a I. Gray, D.G. Watson, J.C. Olivier, W. Couet, I.F. Uchegbu, Niosomes and polymeric chitosan based vesicles bearing transferrin and glucose ligands for drug targeting, Pharm. Res. 17 (2000) 1250–1258, https://doi.org/10.1023/A:1026422915326.
- [103] J. Siepmann, N.A. Peppas, Modeling of drug release from delivery systems based on hydroxypropyl methylcellulose (HPMC), Adv. Drug Deliv. Rev. 48 (2001) 139–157, https://doi.org/10.1016/S0169-409X(01)00112-0.
- [104] F.T. Li, D.S. Zhao, Q.Z. Luo, R.H. Liu, R. Yin, Research on surface-modification of Nano-TiO2 by span 60, J. Ceram. Process. Res. 9 (2008) 398–400.

- [106] M.I. Khan, A. Madni, J. Hirvonen, L. Peltonen, Ultrasonic processing technique as a green preparation approach for diacerein-loaded niosomes, AAPS PharmSciTech 18 (2017) 1554–1563, https://doi.org/10.1208/s12249-016-0622-z.
- [107] B. Nasseri, Effect of cholesterol and temperature on the elastic properties of niosomal membranes, Int. J. Pharm. 300 (2005) 95–101, https://doi.org/ 10.1016/j.ijpharm.2005.05.009.
- [108] S. Islam, M. Haque, A. Bakr, Preparation and characterization of phthalic acid-propane-1, 2- diol-glycerol Co-polyester as A biodegradable polymer, J. Compos. Biodegrad. Polym. 2 (2014) 80–87, https://doi.org/10.12974/2311-8717.2014.02.02.4.
- [109] R.A. Cox, Revised mechanism for the hydrolysis of ethers in aqueous acid, Can. J. Chem. 90 (2012) 811–818, https://doi.org/10.1139/v2012-060.
- [110] H.A. Ayala-Bravo, D. Quintanar-Guerrero, A. Naik, Y.N. Kalia, J.M. Cornejo-Bravo, A. Ganem-Quintanar, Effects of sucrose oleate and sucrose laureate on in vivo human stratum corneum permeability, Pharm. Res. 20 (2003) 1267–1273, https://doi.org/10.1023/A:1025013401471.
- [111] P. Karande, S. Mitragotri, Enhancement of transdermal drug delivery via synergistic action of chemicals, Biochim. Biophys. Acta Biomembr. 1788 (2009) 2362–2373, https://doi.org/10.1016/j.bbamem.2009.08.015.
- [112] M. Fresta, G. Puglisi, Application of liposomes as potential cutaneous drug delivery systems. In vitro and in vivo investigation with radioactively labelled vesicles, J. Drug Target. 4 (1996) 95–101, https://doi.org/10.3109/ 10611869609046267.

- [113] P.L. Honeywell-Nguyen, J.A. Bouwstra, Vesicles as a tool for transdermal and dermal delivery, Drug Discov. Today Technol. 2 (2005) 67–74, https://doi.org/ 10.1016/j.ddtec.2005.05.003.
- [114] F. Larese Filon, M. Mauro, G. Adami, M. Bovenzi, M. Crosera, Nanoparticles skin absorption: new aspects for a safety profile evaluation, Regul. Toxicol. Pharmacol. 72 (2015) 310–322, https://doi.org/10.1016/j.yrtph.2015.05.005.
- [115] J. Lademann, H. Richter, A. Teichmann, N. Otberg, U. Blume-Peytavi, J. Luengo, B. Weiß, U.F. Schaefer, C.M. Lehr, R. Wepf, W. Sterry, Nanoparticles an efficient carrier for drug delivery into the hair follicles, Eur. J. Pharm. Biopharm. 66 (2007) 159–164, https://doi.org/10.1016/j.ejpb.2006.10.019.
- [116] J. Lademann, F. Knorr, H. Richter, U. Blume-Peytavi, A. Vogt, C. Antoniou, W. Sterry, A. Patzelt, Hair follicles - an efficient storage and penetration pathway for topically applied substances, Skin Pharmacol. Physiol. 21 (2008) 150–155, https://doi.org/10.1159/000131079.
- [117] J. Kreuter, Influence of the surface properties on nanoparticle-mediated transport of drugs to the brain, J. Nanosci. Nanotechnol. (2004), https://doi.org/10.1166/ inn.2003.077.
- [118] J. Kreuter, D. Shamenkov, V. Petrov, P. Ramge, K. Cychutek, C. Koch-Brandt, R. Alyautdin, Apolipoprotein-mediated transport of nanoparticle-bound drugs across the blood-brain barrier, J. Drug Target. (2002), https://doi.org/10.1080/ 10611860290031877.

# **Supporting information**

Tailoring Solulan C24 based Niosomes for Transdermal Delivery of Donepezil: *In vitro* characterization, Evaluation of pH sensitivity, and Microneedle-assisted *Ex vivo* Permeation Studies.

Archana S Nayak<sup>1</sup>, Srivani Chodisetti<sup>1</sup>, Shivaprasad Gadag<sup>2</sup>, Usha Yogendra Nayak<sup>2</sup>, Srinikethan Govindan<sup>1</sup>, Keyur Raval<sup>1\*</sup>.

<sup>1</sup>Department of Chemical Engineering, National Institute of Technology Karnataka, Surathkal, Mangalore, 575025, India.

<sup>2</sup>Department of Pharmaceutics, Manipal College of Pharmaceutical Sciences, Manipal Academy of Higher Education, Manipal, Karnataka- 576104, India.

## **Corresponding Author:**

Dr. Keyur Raval,

**Department of Chemical Engineering,** 

National Institute of Technology Karnataka,

Surathkal, India. 575025

phone number: +91 9342421444

email id: keyurnraval@nitk.edu.in

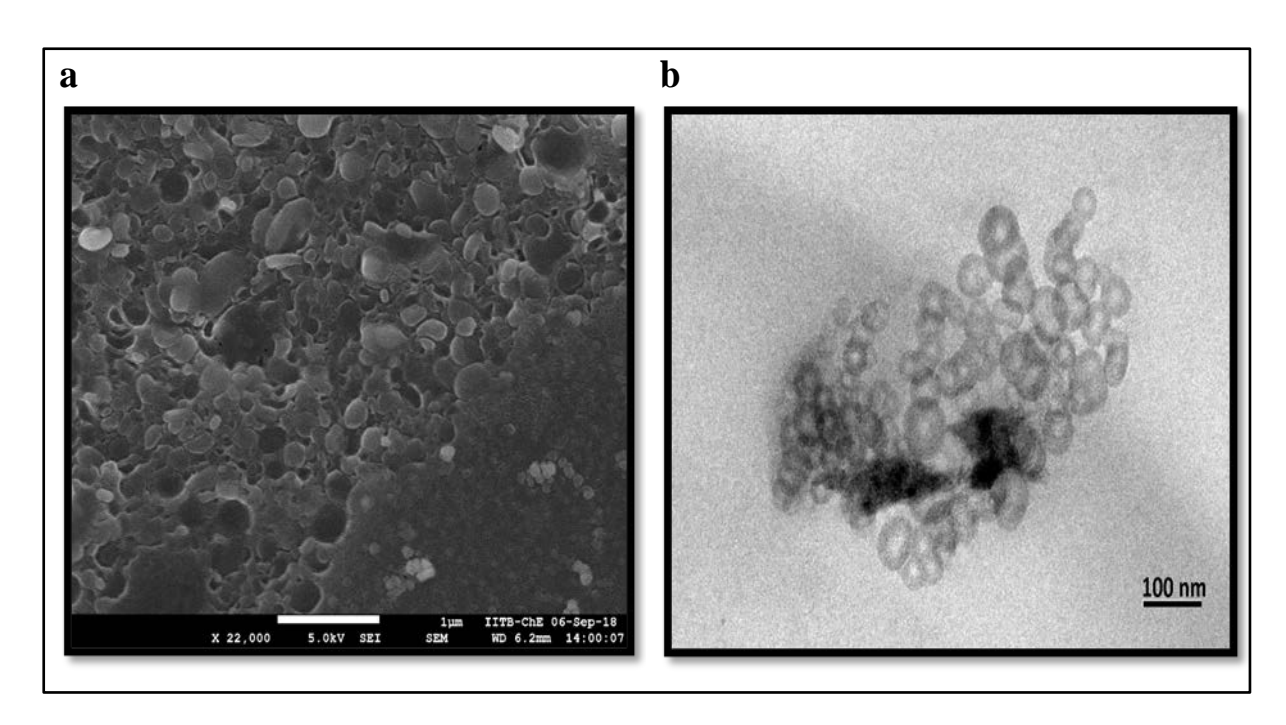


**Figure S1** (a) The cryo-SEM imaging of the NCV1 formulation. (b) The high-resolution TEM imaging of the NCV1 formulation.

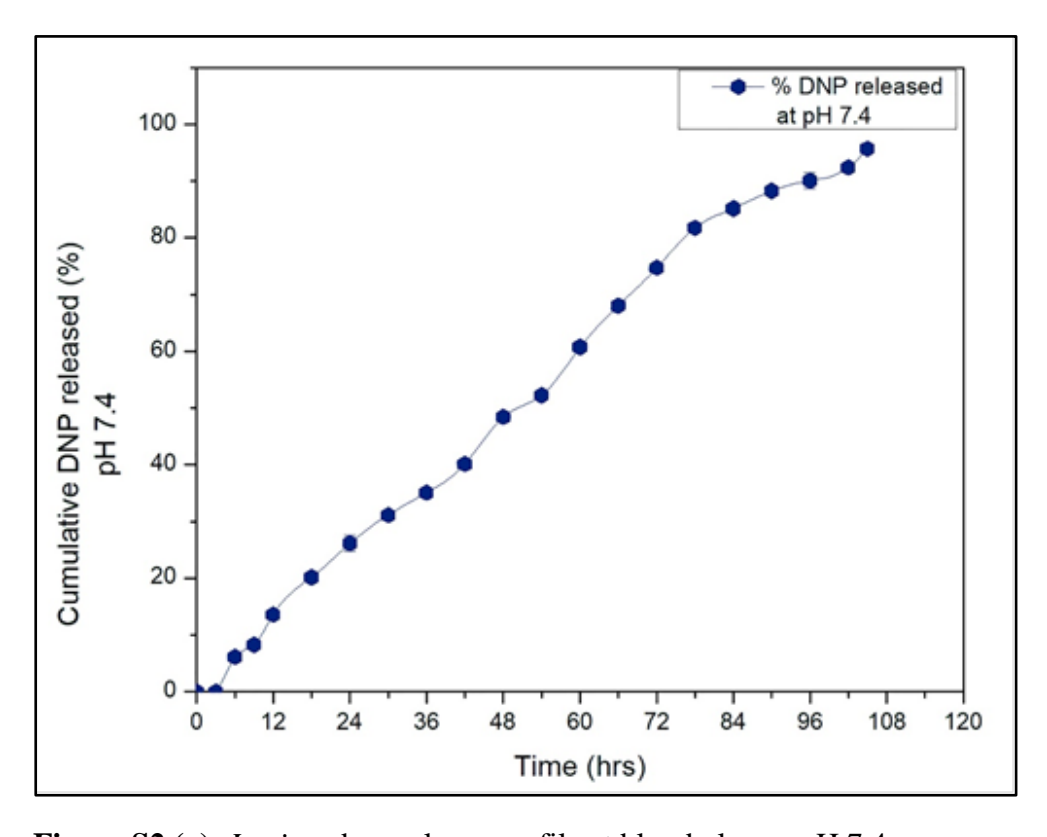


Figure S2 (a): In vitro drug release profile at blood plasma pH 7.4.

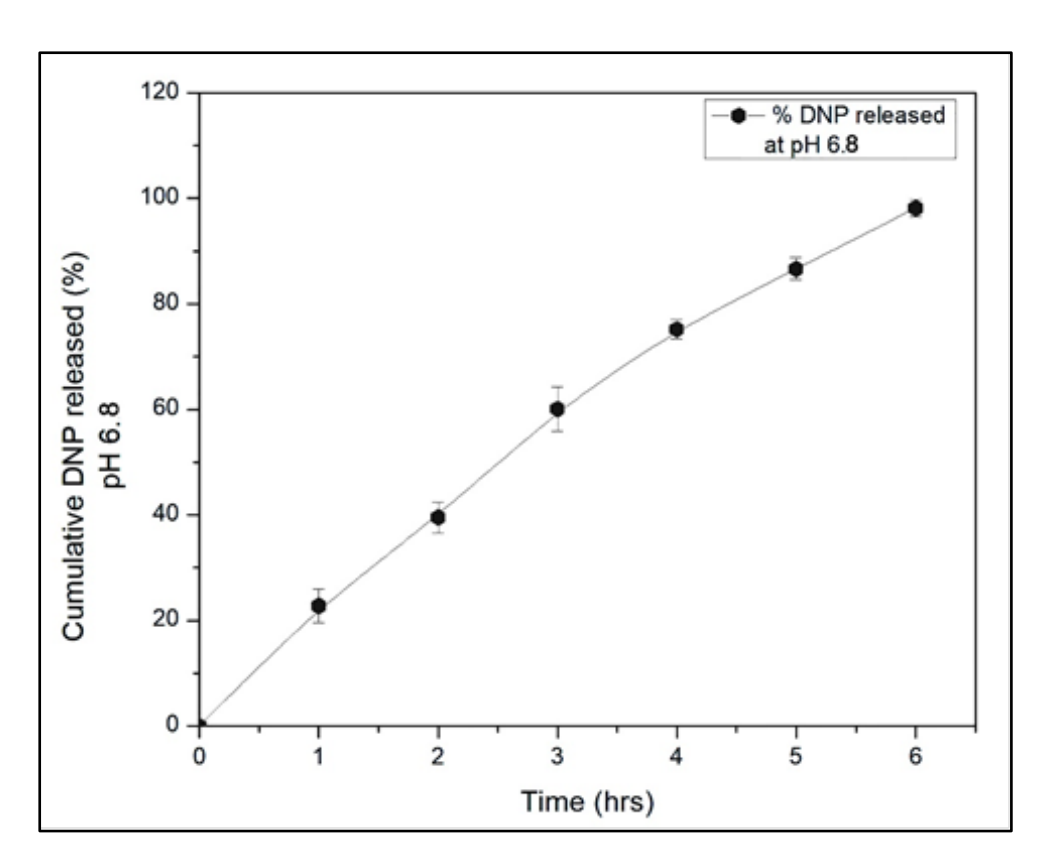


Figure S2 (b): In vitro drug release profile at AD brain pH 6.8.

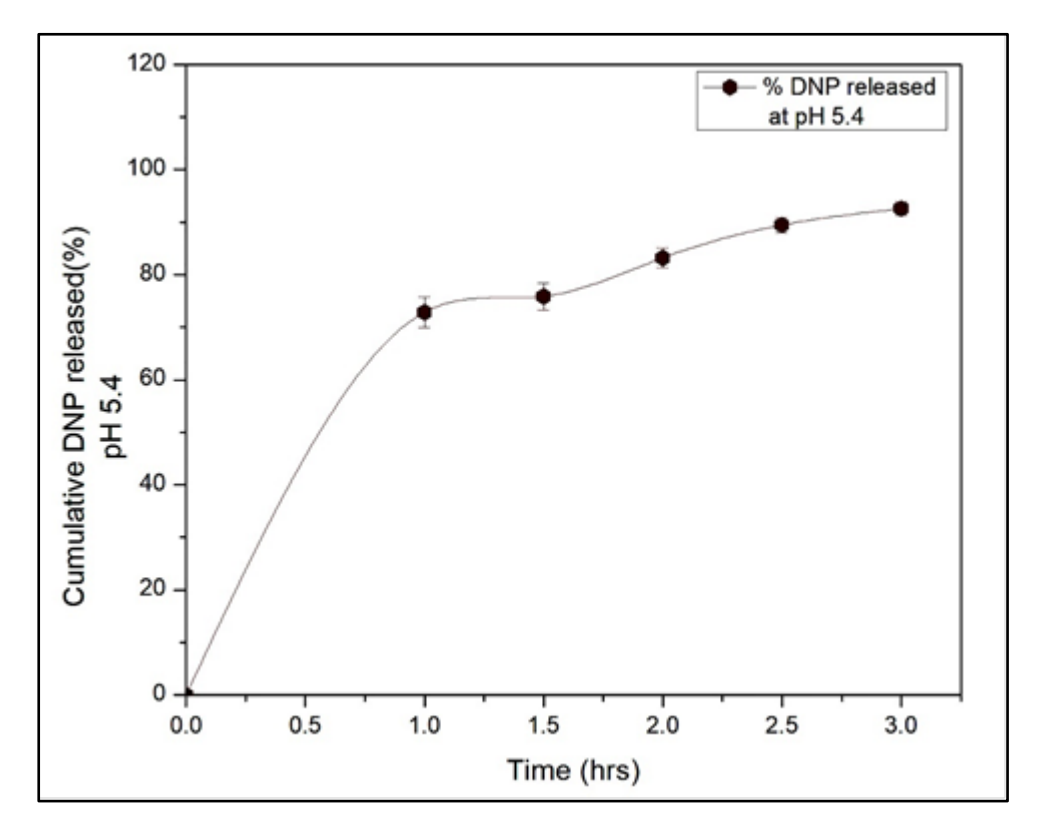
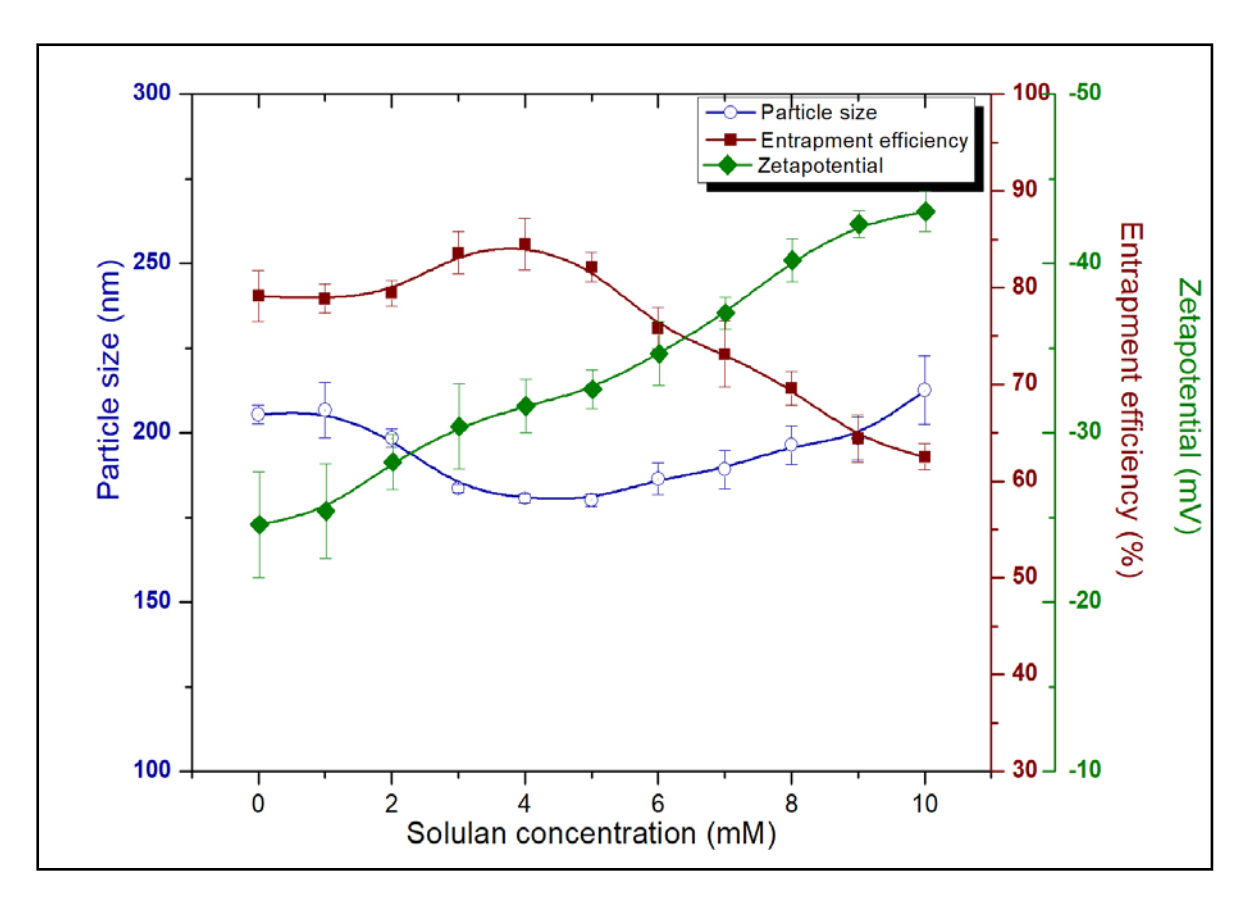
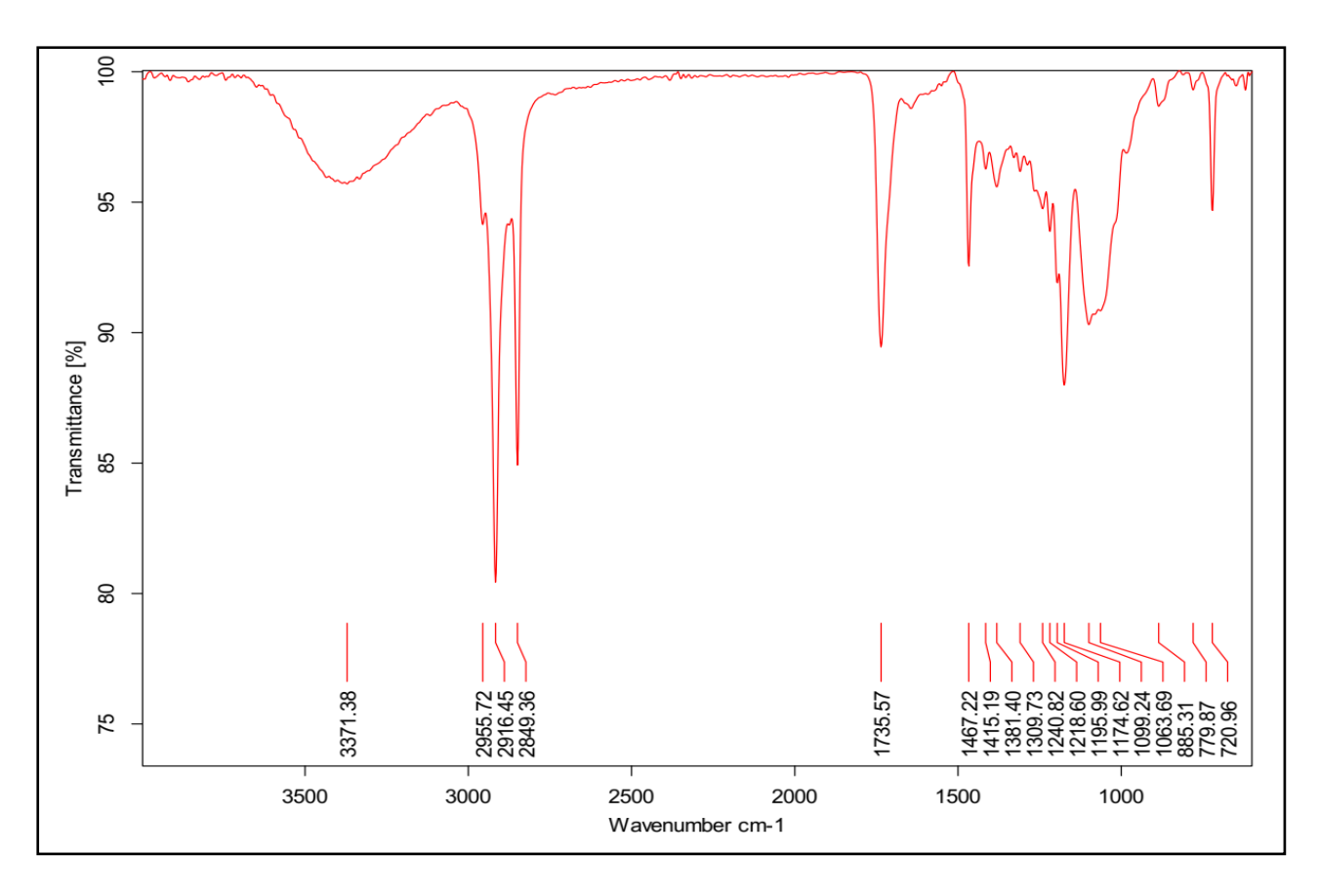


Figure S2 (c): In vitro drug release profile at skin pH 5.4.



**Figure S3.** Effect of increasing Solulan C24 concentration on niosomes size, entrapment efficiency, and zeta potential.



**Figure S4**: FTIR spectra of Span 60

Table S1: Characteristic FTIR peaks of Span 60

Wavenumber	Characteristic peaks	Wavenumber	Characteristic peaks
cm <sup>-1</sup>		cm <sup>-1</sup>	
3371.38	OH broad spectra	1467.22	Deformation peak
			corresponds to C=C
2955.72	Strong assymetric stretching	1381.40	Bend corresponds to O-
2916.45	of aliphatic -CH		CH of the tetrahydrofuran
2849.36			ring
1735.57	In-plane bending vibration of	1174.62	Corresponds to the CH of
1643.96	C=O and rocking vibration of	1099.24	alcohol group
	-O-CH2 corresponds to the		
	ester		

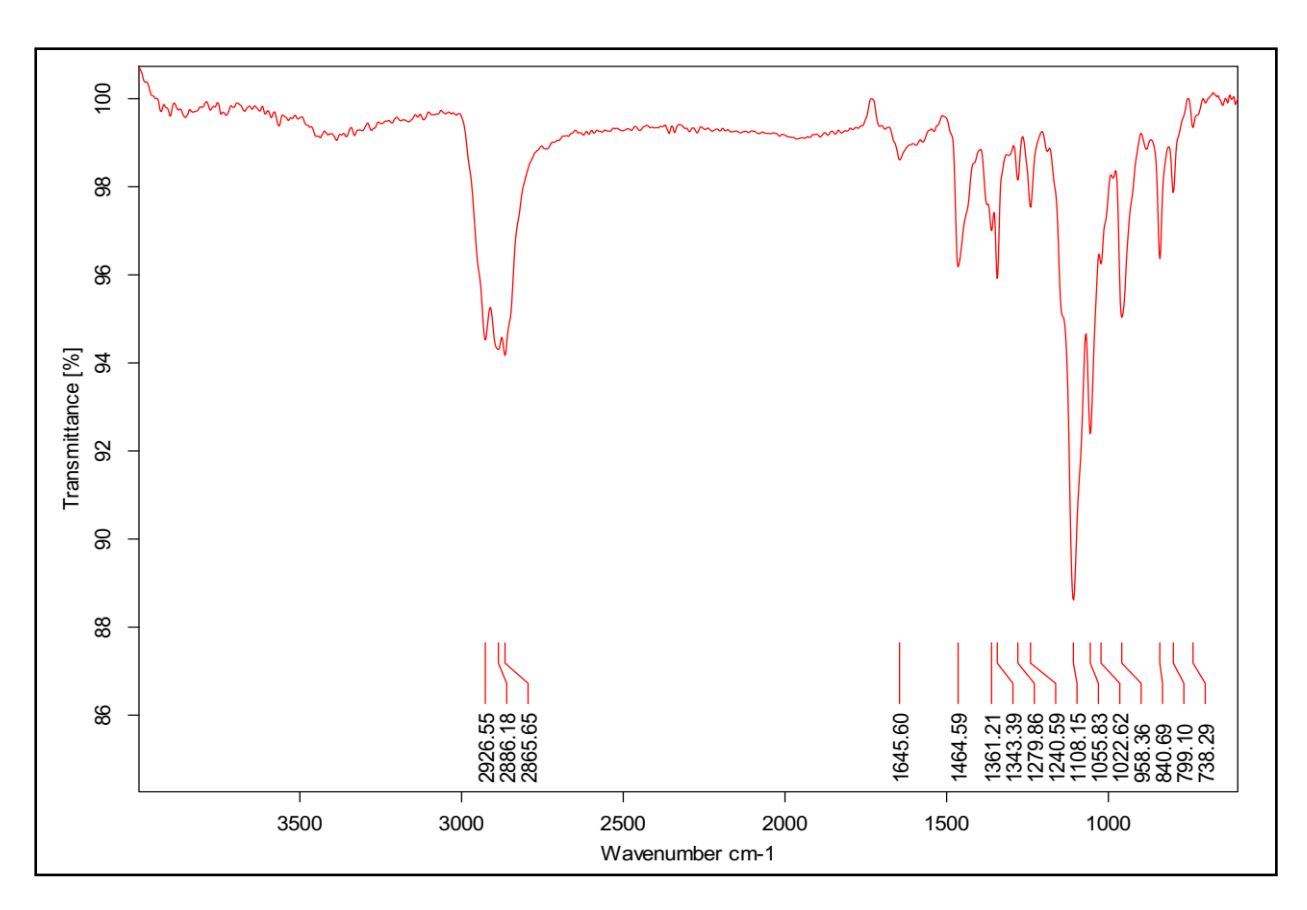


Figure S5: FTIR spectra of Cholesterol and Solulan C24

Table S2: Characteristic FTIR peaks of Cholesterol and Solulan C24

Wavenumber	Characteristic peaks	Wavenumber	Characteristic peaks
cm <sup>-1</sup>		cm <sup>-1</sup>	
22926.55	strong peaks with three bands	1361.21	O-H deformation
2886.18	for –CH <sub>3</sub> and -CH <sub>2</sub>		
2865.65			
1645.60	Weak C=C stretching vibration	1343.39	C-O stretching vibration
	peak		
1464.59	Medium band and a sharp	958.36	Out of plane angular
1108.15	stretching	840.69	deformation for C-H
	Ether of solulan C24		

Figure S6: Chemical structures of Span 60, Cholesterol and Solulan C24.

Table S3: Zeta potential of  $NSV5_{SolC24}$  at different physiological pH.

рН	Zeta potential (mV)
Plasma, pH 7.4	-32.7±1.17
Brain, pH 6.8	-28.5±2.33
Skin, pH 5.4	-21.42±1.86